The Fermilab Holometer

A program to measure Planck scale indeterminacy

Aaron Chou, Craig Hogan (Spokesperson), **Erik Ramberg**
Jason Steffen, Chris Stoughton, Ray Tomlin, William Wester
Fermilab Center for Particle Astrophysics

Sam Waldman, Rainer Weiss
Massachusetts Institute of Technology

Stephan Meyer
University of Chicago

H. Richard Gustafson
University of Michigan

Stanley Whitcomb
California Institute of Technology

Abstract

We propose an experiment at Fermilab to study a conjectured effect called "holographic noise" that may arise from new Planck scale physics: the measured positions of bodies may wander randomly from ideal geodesics of classical relativity, in measurement-dependent directions, by about a Planck length per Planck time. The experiment will search for this holographic jitter in the relation of mass-energy and space-time by looking for correlated phase noise between two neighboring 40 meter interferometers. The goal of the experiment is to provide convincing evidence for or against the hypothesis that relative transverse positions of bodies display this particular new kind of quantum noise, whose power spectrum is independent of frequency and has a spectral density determined only by the Planck time. A positive result of the experiment would be a major step forward in understanding the emergence of space-time and mass-energy from a unified theory of spacetime and quantum mechanics. A negative result will impact the macroscopic interpretation of unified theories.

Contents

List of Figures

A Introduction

This document is a proposal for an experiment at Fermilab to study a new conjectured physical effect called "holographic noise". The goal of the experiment is to provide convincing evidence for or against the hypothesis that relative transverse positions of bodies display a particular new kind of quantum noise, whose power spectrum is independent of frequency and has a spectral density determined only by the Planck time. It could be described as the first high-frequency, time-resolved test of the equivalence principle with Planck sensitivity. A positive result of the experiment would be a major step forward in understanding the emergence of spacetime and mass-energy from unified theory. A negative result will impact on the macroscopic interpretation of unified theory.

We plan to build two 40-meter power-recycled Michelson interferometers to be used in close proximity to each other. The signals from the dark ports of the two interferometers will be cross-correlated at frequencies up to 4 MHz, corresponding to the round trip light travel time. Separate lasers, vacuum systems, and detectors will be used for each interferometer so that conventional noise from these two completely independent systems can grow by at most the square root of integration time in the cross-correlation function. However, if holographic noise exists and causes a common jitter in the underlying space-time neighborhood that the two interferometers co-occupy, then the two devices will see this common source of noise. This correlated phase noise adds coherently in the cross-correlation function and grows linearly with integration time. It can be measured with $\approx 5\sigma$ significance relative to the uncorrelated noise sources after 1.5 hours. The interferometers will be designed in such a way that, if there is a positive signal, they can be moved relative to each other to test the predicted variation of holographic correlation with space-time separation. The interferometers will likely be deployed in large leased space to allow these reconfigurations.

Once the project is approved, we plan to prepare a Field Work Proposal to obtain funding from DOE. The construction cost (exclusive of scientist effort) is estimated to be under \$2M, and is dominated by procurements for optics, electronics, and mechanical components. The estimated lead times for these purchases are all 10 weeks or shorter, so we allocate three months to the construction phase, which ends when all of the components are available "on the floor" of the operations space. For operations, we plan on six months to commission the interferometers, followed by up to 2.5 years to measure holographic noise and study systematic effects.

A.1 Holographic noise prediction

The notion of a spacetime event is not easily interpreted in the context of quantum mechanics. For one thing, the notion of a pointlike event does not take account of the particle/wave duality of quantum mechanics. For another, events themselves are not, even in principle, observable quantities, but are measured only by interactions of mass-energy. These issues, although studied for many years, still present a challenge to any theory that seeks to unify spacetime with mass-energy and quantum theory.

For example, one well known paradox is that no quantum particles can exist in classical, 3+1D spacetime above the Planck energy, because of gravity. A state of a particle spatially localized within a Planck volume lies within the Schwarzschild radius for its energy, behind an event horizon where it can never be seen. Some unified theories suggest that beyond the

Planck time, $\lambda_P/c \equiv t_P \equiv \sqrt{\hbar G_N/c^5} = 5.4 \times 10^{-44}$ seconds, physics changes character in some fundamental way, so that a 3+1D spacetime effectively behaves like it has a minimum length or a maximum frequency at the Planck scale. Precise results from black hole evaporation physics, a theoretical bridge between classical spacetimes and quantum particle states, also suggest a fundamental bound at the Planck scale.

We adopt a particular hypothesis about this bound that has macroscopically measurable consequences. Specifically, we identify the Planck scale as a maximum frequency in any frame, and then assert that observable relative positions of bodies in that frame are entirely defined by wavefunctions with the Planck frequency limit. The paths that connect events and the relationships of bodies in classical spacetime then have the same status as rays in optics: they are an approximate description of a configuration of a system of waves. Rays have a fundamental indeterminacy imposed by diffraction limits; their position and direction are not uniquely determined. The actual physical system, consisting of wave energy (or in this application, position probability), is not sharply confined into classical lines and points. A time-averaged classical metric does not capture these wavelike qualities. Just as in wave optics, diffractive blurring of position in such a system can occur on observable scales much larger than the Planck length, given a macroscopic propagation distance to provide a suitably long lever arm.

Specifically, we assert that information in measurable correlations between observables at two events is limited to information that can be carried on Planck wavelength null fields over a light cone that includes both events, and that correlations of position observables are described by a simple effective theory based on wave optics (Hogan, 2008a,b; Hogan and Jackson, 2009; Hogan, 2009). The new indeterminacy arises because the wavefunction encoding the transverse component of position spreads by diffraction. Just as in diffraction of classical waves, the resulting transverse position uncertainty of a system satisfies

$$\sigma(L) \geq \sqrt{\lambda_0 L/(2\pi)} \tag{1}$$

after longitudinal propagation over a length L, if this transverse information is encoded with minimum wavelength $\lambda_0 = 2\lambda_p$. The normalization of the minimum wavelength is implied by the black hole entropy-area relationship $S = A/4G_N = A/(2\lambda_p)^2$.

In the context of an interferometer, measurement of a phase signal collapses the position wavefunction of the underlying space-time. Random mode phases of waves with different frequencies lead to an indeterminate outcome that varies with time. The variations add a new kind of Planck amplitude noise to the signal like a bounded random walk of the beamsplitter. During the time it takes light to traverse an arm, the beamsplitter "wanders" transversely over a spatial interval approximately given by the geometric mean of the apparatus size and the Planck length. The wandering is correlated for nearby interferometers to the extent that their light cones overlap, because they must collapse into the same states.

The effective theory of holographic noise based on the above principles is precisely calibrated using black hole entropy, and gives zero-parameter predictions (Hogan, 2009) for observables such as the frequency spectrum of phase noise, as well as estimates for the cross-correlation of two close-by interferometers.

Specifically, for a single interferometer, the noise is characterised by the time autocorrelation of $X(t)$, the pathlength difference between the waves from the two arms. The autocorrelation

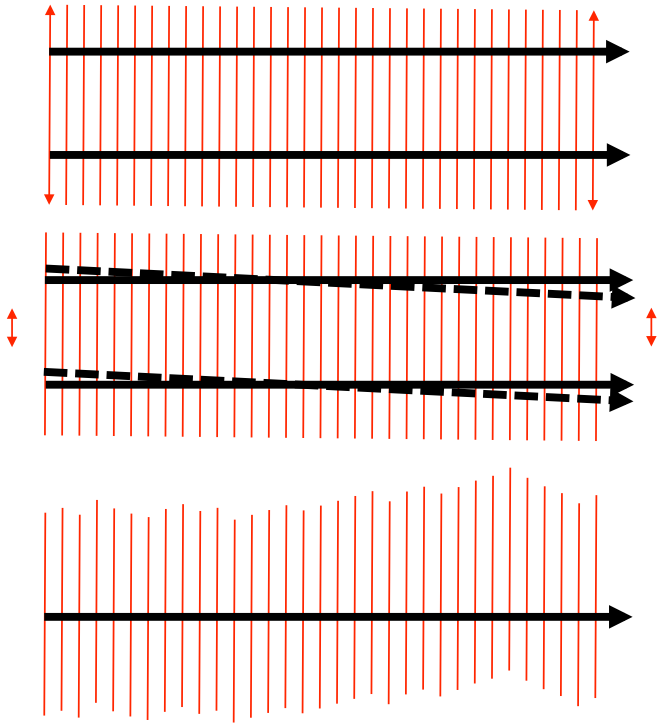

Figure 1: A summary of the holographic uncertainty hypothesis.
Top panel: A set of null wavefronts of infinite transverse extent with wavelength $2\lambda_P$ defines a precise direction in space, a family of parallel paths. Plane waves in three dimensions can be used to define a classical spacetime at Planck resolution in three dimensions. The exact wavelength is chosen to match the known information capacity of a black hole event horizon.
Middle panel: Suppose spatial positions of bodies are encoded on the wavefronts. Transverse localization (within a wavefront) corresponds to a spatial wavepacket of a certain width, as indicated by the small vertical arrows. If the positions are localized on any wavefront, then the resulting transverse momentum spread (due to the Heisenberg uncertainty principle applied to Planck wavelengths) causes an uncertainty in angle, or in relative positions on different wavefronts. Transverse localization thus corresponds to a superposition of different rays, or families of paths. In each family the paths are still nearly parallel but differ from the classical reference spacetime of the first panel. In reality the transverse coherence falls off on a scale comparable to the path length, as the paraxial approximations break down.
Lower panel: When a measurement of transverse position is made, it fixes a classical transverse position, chosen from the distribution described by the transverse wavefunction. Relative to the reference spacetime, a continuously measured transverse position appears to execute a random walk of about Planck length per Planck time, shown here as a wandering of matter in the wavefront plane. In an interferometer of size L, the random walk seen in the signal is bounded by the time $2L/c$, because wavepacket spreading over longer time intervals is not measured. In other words, on short time scales less than the light travel in the arms, the beamsplitter has a transverse jitter with respect to the beam coming from the end mirror, but on longer time scales, the beamsplitter and end mirror undergo a common correlated transverse motion.

is defined as the limiting average,

$$\Xi(\tau) = \lim_{T\to\infty} (2T)^{-1} \int_{-T}^{T} dt X(t) X(t+\tau) \tag{2}$$

The semiclassical theory gives a prediction for this quantity,

$$\Xi(\tau) = \frac{\lambda_p}{\pi}(2L - c\tau), \qquad 0 < \tau < 2L/c, \tag{3}$$

and

$$\Xi(\tau) = 0, \qquad \tau > 2L/c. \tag{4}$$

In the frequency domain, the power spectral density of displacement is defined as $\tilde{\Xi}(f) = 2\int_0^\infty d\tau \Xi(\tau)\cos(\tau\omega)$, where $\omega = 2\pi f$. The prediction for the frequency spectrum of the holographic displacement noise is then

$$\tilde{\Xi}(f) = \frac{c^2 2t_P}{\pi(2\pi f)^2}[1 - \cos(f/f_c)], \qquad f_c \equiv c/4\pi L. \tag{5}$$

Note that this predicted spectrum is valid at all frequencies for a given interferometer of length L. In the low frequency limit, the spectrum is independent of f:

$$\tilde{\Xi}(f) \approx 4t_P L^2/\pi, \qquad f << c/2L. \tag{6}$$

To obtain the apparent gravitational wave dimensionless strain power spectral density, for a simple Michelson interferometer, this expression should be divided by L^2. For other configurations, the translation is more complex.

A key element of our experimental design is the correlation of the noise signals in two separate interferometers. This noise correlation is expected if two devices are located sufficiently closely such that the jitter in the underlying spacetime is causally correlated. In the holographic effective theory built on light sheets, time and longitudinal position are identified. Measurement of a position at one point on a light sheet collapses the wavefunction at other points on the wavefront, even though they have spacelike separation. The apparent motion is thus in common across a significant transverse distance— not only across a macroscopic beamsplitter, say, but even between between disconnected systems. This correlation has the same character as other quantum correlations between spacelike-separated measurements: the correlation is limited by causality. In the interferometers, where two longitudinal directions are being compared, the measured phase difference in one interferometer is correlated with a portion, but not all of the phase difference in another, nearby interferometer. The future light cone of a reflection event along one arm, and the past light cone of the reflection event along the other arm, define a causal diamond; the signal is not correlated with systems beyond this volume of spacetime.

For small displacements of two aligned interferometers offset along either arm by ΔL, the cross correlation of effective beamsplitter position is estimated to be

$$\Xi_\times(\tau) \approx (\lambda_P/\pi)(2L - 2\Delta L - c\tau), \qquad 0 < c\tau < 2L - 2\Delta L \tag{7}$$

$$= 0, \qquad c\tau > 2L - 2\Delta L. \tag{8}$$

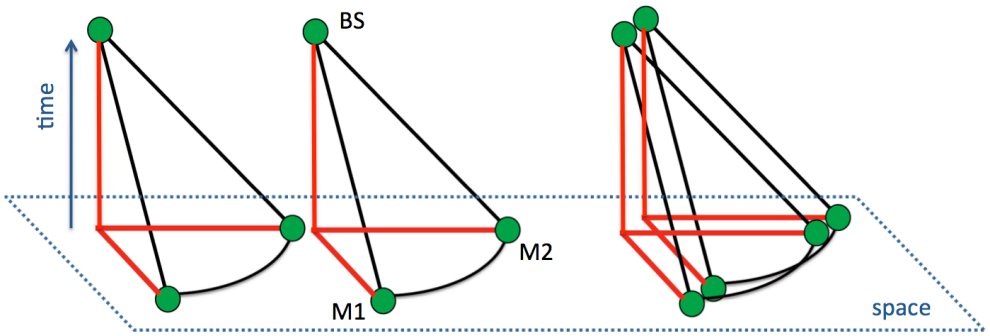

Figure 2: Neighboring interferometers will experience correlated phase noise if the causal light cones of the reflection events in each device have significant overlap. In this diagram, the horizontal plane represents the plane of the interferometer arms, and the vertical axis represents time. The green dots represent reflection events at the beamsplitters, BS, and the end mirrors, M1 and M2. The causal diamond is the intersection of the past light cone of one beamsplitter reflection event, shown here, and the future light cone of another (the reflection of the cones drawn here through the horizontal plane). The measured signal is only correlated with events in the enclosed spacetime volume. On the left, the two interferometers are separated and their causal diamonds do not overlap. The space-time wavefunctions of the two beamsplitter positions collapse into independent states when the dark port photons are measured, and there is no correlation between the phase noise seen in each interferometer. On the right, for two neighboring interferometers, the spacetime volume enclosed by the causal diamond overlaps considerably, so the two beamsplitter wavefunctions collapse into nearly the same space-time state and their random walks are highly correlated. The resulting correlated phase noise is expected to decrease monotonically as the two interferometers are moved apart.

In the frequency domain, the low frequency limit of cross-correlation becomes

$$\tilde{\Xi}_{\times}(f) \approx 4t_P L^2[1-(\Delta L/L)]/\pi, \qquad f << c/2L. \tag{9}$$

The holographic interferometer experiment proposed here tests these predictions. Either a positive or a null result should throw light on the little understood macroscopic classical limit of unification theories.

A.2 Comparison with other experiments

No experiment has yet been done to search specifically for holographic noise. However, two existing gravitational wave interferometers may be capable of detecting the effect as a new noise source, and we have obtained information about their results.

The GEO-600 interferometer has had "mystery noise" which has limited their strain sensitivity for about two years. The holographic prediction approximately accounts for all of the unexplained noise at frequencies above about 500Hz, its most sensitive frequency. At that frequency, the mystery noise is about 30 percent of the total noise. GEO600 is in the process of making an accounting sum of several noise terms. Hopefully these terms will be well understood and small enough so that errors in them will not mask the holographic noise. However, there is no guarantee of this, and systematic uncertainties could limit the ability of GEO600 to make a convincing detection or exclusion of the predicted effect. Unlike the currently proposed experiment, it is not designed to isolate signatures of the holographic noise effect.

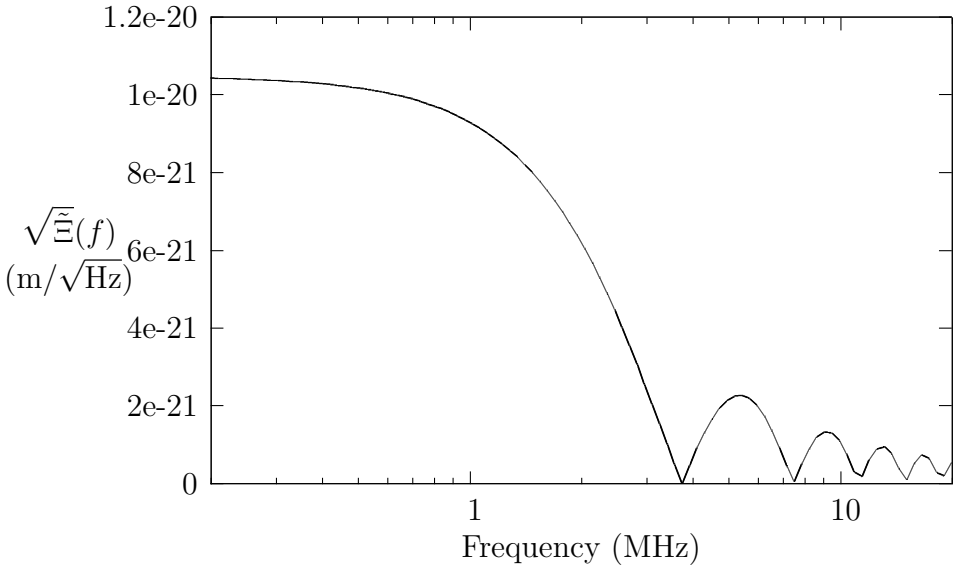

Figure 3: Predicted frequency spectrum of holographic noise displacement $\sqrt{\tilde{\Xi}(f)}$ for a single Michelson interferometer with L=40m. Because the holographic signal (Equation 5) adds in quadrature to the noise of a single interferometer and is subdominant, this spectrum is difficult to measure cleanly in an individual interferometer. Instead, we will measure the cross-correlation of the noise $\tilde{\Xi}_\times(f)$ (Equation 9) in two interferometers operated in close proximity. The component of the noise product due to the holographic jitter of the common underlying spacetime will sum coherently and grow linearly with time, while the product of the uncorrelated random noise in the two devices will sum with a random phase and grow only as the square root of time. In this way, the correlated noise can be easily isolated. For $\Delta L \to 0$, the normalization $\tilde{\Xi}_\times(f) = \tilde{\Xi}(f)$. Using 1064 nm photons, the corresponding phase noise spectral density is $\Phi_{\text{holo}} \approx 6 \times 10^{-14}$ radians/$\sqrt{\text{Hz}}$, a level easily probed with a modest requirements on interferometer design and integration time.

Very recently, the mystery noise at lower frequencies in GEO600 has been accounted for. Most of the larger amplitude, low frequency noise between 100 to 300Hz is believed to be due to AM on the RF sidebands used in the fringe interrogation. However, the lower amplitude mystery noise is still present at higher frequencies, with approximately Planck amplitude.

Because of a different optical design, the LIGO interferometers do not have the same sensitivity for a beam splitter motion as for an arm length change. The arm length change defines the sensitivity of the instrument for gravitational waves and is enhanced by using optical cavities in the arms. One needs to have approximately 200 times larger motion of the beam splitter than of an arm cavity mirror to achieve the same interferometer output signal. The two nearly-colocated LIGO interferometers, H1 and H2, at Hanford, Washington, have been cross correlated in the S5 one year run. Preliminary results in the 400 to 1000 Hz band have a noise limit comparable to the predicted holographic noise for a single interferometer. (These results are planned to be published in 2010 but have been discussed at LIGO Scientific collaboration meetings in 2009). A careful estimate of the expected holographic noise in this cross correlation needs to be carried out as the geometry of interferometer paths and the role of the optical cavities complicates the interpretation of the result. Initial thinking is that the H1 and H2 geometric configuration has reduced sensitivity to the holographic noise so this limit will not be competitive. In any case there is no expectation of improvements in the LIGO results until the commissioning of the third interferometer in advanced LIGO in about 4 to 5 years. This could allow renewed correlation measurements below 10kHz. However, at these low frequencies, there is still a chance for correlation between the H1 and H2 due to environmental causes.

The current proposal is to carry out a unique experiment that is not being done anywhere else–one that is optimized to search for holographic noise rather than for gravitational waves. The experiment is designed to look at the direct correlation of two isolated interferometers at MHz frequencies where the probability of environmental or accidental correlations between the interferometers is anticipated to be small and easily measurable. The correlation will be done with frequency resolution (crosspower spectra) so that accidental correlations at specific RF spectral lines (such as radio stations and other remaining radio frequency interference) can be identified. Furthermore, the ability to move the two interferometers apart allows further tests of specific predictions of the causal model of holographic noise correlations. For example, the correlated noise signal is expected to decrease monotonically as the beamsplitters in the two devices are moved apart.

A.3 Proposed measurement technique

The proposed experiment will search for correlations in the noise signals observed in two neighboring interferometers, induced by jitter in the underlying space-time. The jitter is expected to be highly correlated between two interferometers in close physical proximity since it is a property of the space-time through which the photon beams are propagating, and not specifically a property of the individual photon beam. In the cross-correlation of the two noise signals, the correlated noise product will grow linearly with time while the uncorrelated noise product will enter with a random sign and grow only with the square root of time. This fact will allow us, with sufficient integration time, to extract the correlated noise component even if it only forms a small fraction of the total noise.

We will study several signatures of the correlation of holographic noise. We will measure how the correlation depends on time lag and frequency, the separation between the interferometers, and the angle between the orientations of the interferometers.

Equation 8 predicts the shape of the correlation function in the time domain, shown in Figure 4. Equation 8 also predicts reduced correlation at all time lags as the separation between the two interferometers varies, shown here for $L = 40$ meter arm lengths.

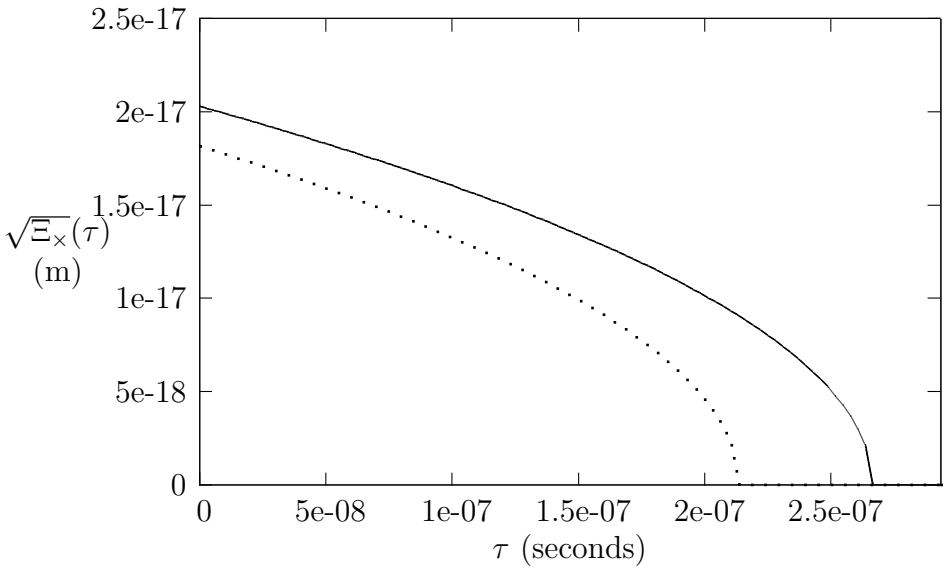

Figure 4: Predicted cross correlation in the time domain between two $L = 40$ meter interferometers, for two different configurations. The shape of the correlation is an important diagnostic. The solid line is for an offset $\Delta L = 0$, while the dotted line is for $\Delta L = 8$ meters. Note that the exact shape of Equation 8 is only valid for $\Delta L \to 0$. Causality arguments predict that the correlation falls to zero for $\Delta L \geq L$.

General arguments also suggest that the cross correlation is maximum for aligned interferometers, $\Delta_\theta = 0\,^\circ$, and decreases to zero for $\Delta_\theta \geq 90\,^\circ$. This happens because the signal of each is only sensitive to components of effective motion normal to the plane of each beamsplitter. Assuming that the interpolation between $0\,^\circ$ and $90\,^\circ$ scales as $\cos(\Delta_\theta)$, we expect to see the correlation vary as shown in Figure 5.

The initial stage of the experiment is to measure the cross correlation between two aligned, closely-spaced interferometers ($\Delta L << L$), and see whether $\Xi_\times(\tau)$ has the magnitude and shape given by Equation 8 in the time domain, and $\tilde{\Xi}_\times$ has the magnitude given by Equation 9 in the frequency domain. A positive correlation signal in just this configuration is not convincing, since there may be various, probably electromagnetic, sources of correlation. Most of the effort during the initial operation period of this experiment is expected to be devoted to detective work to track down and mitigate conventional sources of noise correlation. A result consistent with zero cross correlation in this configuration will allow upper limits to be set on any holographic noise contribution.

In the case of a positive correlation signal, a building sufficiently large to allow reconfigurations allows us to measure the decoherence as a function of ΔL and Δ_θ. Changing Δ_θ

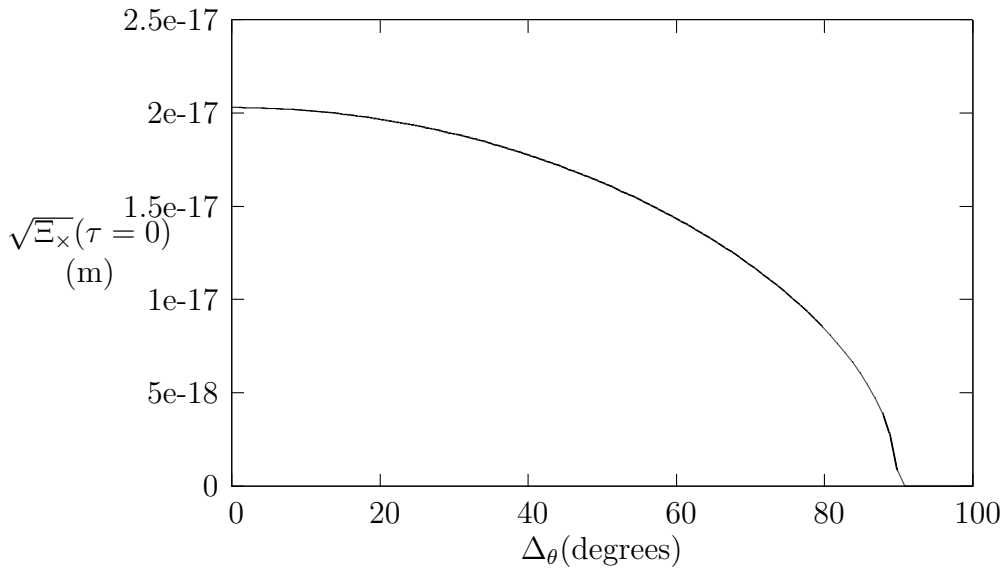

Figure 5: Cross correlation of the holographic signal for 40 meter interferometers with nearly coincident beamsplitters, rotated relative to each other by Δ_θ. Theory predicts reduced cross correlation as they are rotated from $\Delta_\theta = 0\,^\circ$, going to zero for $\Delta_\theta \geq 90\,^\circ$. We plot the interpolation here as $\cos(\Delta_\theta)$.

has the advantage of keeping the spatial separation between the beam splitters and signal photodiodes nearly constant, while modulating the cross correlation. Changing ΔL tests another independent, specific prediction for modulation. In the second stage of the project we will use these experimental signatures to modulate the correlated signal to demonstrate that the signal is not dominated by uncontrolled systematic effects.

B Experimental Design

Initial estimates using two, cross-correlated power recycled Michelson interferometers give an observation time of minutes to achieve unity signal to noise of the holographic noise phase fluctuations against the phase fluctuations due to the Poisson noise of the light. The correlation of the interferometer outputs is done at frequencies larger than 10 kHz where the classical measurement noises are negligible relative to the intrinsic photon phase and amplitude noise.

Known correlated noise above 10 kHz may arise from fluctuations in residual gas density, from optical scattering, and RF pickup in the electronics. This concept uses separate vacuum systems and separate light sources for the two interferometers to reduce the first two noises. One still needs to take care in avoiding light from one interferometer from entering the other and to avoid common excitation of scattering resulting from high frequency acoustic noise on the interferometer tubes and optics. Correlated RF pickup is reduced by careful shielded electronics design.

This design is based on the idea that holographic noise causes phase fluctuations at the output of the two neighboring interferometers which are correlated, and that an independent sample

of the holographic noise is obtained every $2L/c$ seconds. The cross correlation of the phase fluctuations remains constant as the uncorrelated noise is reduced by the square root of the number of independent samples of the cross correlation.

The phase at each individual interferometer output is

$$\phi_1 = \phi_{\rm n1} + \phi_{\rm H} \tag{10}$$
$$\phi_2 = \phi_{\rm n2} + \phi_{\rm H}, \tag{11}$$

where ϕ_{n1} and ϕ_{n2} are the incoherent photon shot noises for each interferometer, and $\phi_{\rm H}$ is the holographic noise. Neglecting cross terms, the cross correlation at zero delay averaged over N samples is approximated by

$$(\phi_1 \times \phi_2)_N = \frac{(\delta\phi_n)^2}{\sqrt{\frac{t_{\rm obs}}{\tau_{\rm sample}}}} + (\delta\phi_{\rm H})^2 \tag{12}$$

where it is assumed that the independent phase noise in the two interferometers has the same variance. $N = t_{\rm obs}/\tau_{\rm sample}$ is the total number of samples in the measurement for an observation time $t_{\rm obs}$. An estimate for the observation time required to have the correlated variances be equal to the uncorrelated one is when the two terms in the cross correlation become equal

$$t_{\rm obs} > \tau_{\rm sample} \left(\frac{(\delta\phi_n)^2}{(\delta\phi_{\rm H})^2} \right)^2 . \tag{13}$$

If the dominant independent noise comes from intrinsic quantum phase fluctuations of the light (a Glauber state for the electromagnetic field of the laser which has a Poisson distribution in photon number and satisfies a photon number-phase uncertainty relationship $\delta\phi \times \delta n \approx 1$), the variance in the phase in a sample $2L/c$ long is

$$(\delta\phi_n)^2 = \frac{1}{n} = \frac{1}{\dot{n}\tau_{\rm sample}} = \frac{hc^2}{2P_{\rm BS}L\lambda_{\rm opt}} \tag{14}$$

where n is the number of photons, $P_{\rm BS}$ is the optical power at the symmetric port of the beam splitter and $\lambda_{\rm opt}$ is the wavelength of the light. This equation determines the design of the experiment. To achieve unity signal to noise, the observation time is

$$t_{\rm obs} > \left(\frac{h}{P_{\rm BS}} \right)^2 \left(\frac{\lambda_{\rm opt}}{\lambda_{\rm Pl}} \right)^2 \left(\frac{c^3}{32\pi^4 L^3} \right). \tag{15}$$

We choose readily achievable parameters (standard within the gravitational wave community) for our benchmark design: $L = 40$ m, $\lambda_{\rm opt} = 1064$ nm and $P_{\rm BS} = 2000$ watts. With these parameters, each interferometer achieves a phase noise sensitivity of $\phi_n(f) = 8 \times 10^{-12}$ radians/$\sqrt{\rm Hz}$. The sampling time is $2L/c = 270$ ns. For predicted holographic phase noise levels (see Figure 3 and appendix H) around $\phi_{\rm holo} \approx 5 \times 10^{-14}$ radians/$\sqrt{\rm Hz}$, Eq. 13 indicates that the observation time to achieve a signal to noise of unity is 3 minutes. Approximately 1/2 hour is needed to achieve a 3 sigma result in the holographic noise power.

The Garching 30 m and Caltech 40 m interferometer exceeded this phase sensitivity by an order of magnitude more than 20 years ago (Shoemaker et al., 1988; Zucker, 1992). In fact, the gravitational wave problem is far more difficult than the interferometry required to detect holographic noise because of the focus on low frequencies. By ignoring the noise below 10 kHz, and focusing on holographic noise at higher frequencies, our holometers avoid the problems with thermal, seismic, and acoustic noise that dominate gravitational wave detector commissioning time. The detector construction is further simplified by the use of standard components for the lasers, optics, mounts and vacuum systems. Indeed, the holometer's size, complexity and sensitivity are quite modest when compared to the prototypes from the gravitational wave community.

Moreover, by using the cross-correlation technique, the correlated phase noise which forms a small fraction of the total shot-noise-dominated phase noise can be robustly isolated. This technique compares favorably to a single interferometer scheme in which various systematic uncertainties (laser power, efficiencies, gains) would have to be understood at the percent level to be able to convincingly measure small excesses in noise above the shot noise expectation.

C Interferometer design

C.1 Power Recycled Interferometer

A power recycled Michelson interferometer senses the beam splitter motion as shown schematically in Figure 6. The Michelson topology senses only the differential motion of the beam splitter while rejecting laser noise. The Michelson is operated close to a dark fringe: the arm lengths are controlled using feedback so that light from the two arms destructively interferes at the beam splitter's output port. The constructive interference at the input port looks, in effect, like a high reflector returning the light from the arms to the laser. The power recycling mirror (PRM) resonates the returned beam, storing the light in the interferometer and multiplying the power incident on the beam splitter for a fixed laser power. The power recycled topology enables the 2 kW of laser power incident on the beam splitter required for reasonable integration times using low power commercial lasers.

The interferometer has two length degrees of freedom, the common arm motion (CARM) and the differential arm motion (DARM). The CARM error signal is derived from a Pound-Drever-Hall style RF detection at the REFL port using 25 MHz RF sidebands. The DARM error signal is derived using DC readout at the AS port, in which a small offset is intentionally introduced into the DARM length. The offset provides a static DC field so that there is a linear coupling of length to intensity at the interferometer output. In Figure 6, the output port has two photo-diodes for diagnostic purposes and for power handling.

The interferometer has been modelled with the Optickle software package, paying particular attention to the DC offset and the PRM transmission. The Optickle input parameters are given in Table 1, note that a small arm length asymmetry is assumed in order to include the effect of laser noise couplings. Figure 7 shows the variance of key interferometer parameters as a function of the PRM transmission, T_{PRM}, and the static DARM offset, δx. The interferometer noise floor is determined by the quadrature sum of shot noise, Johnson thermal

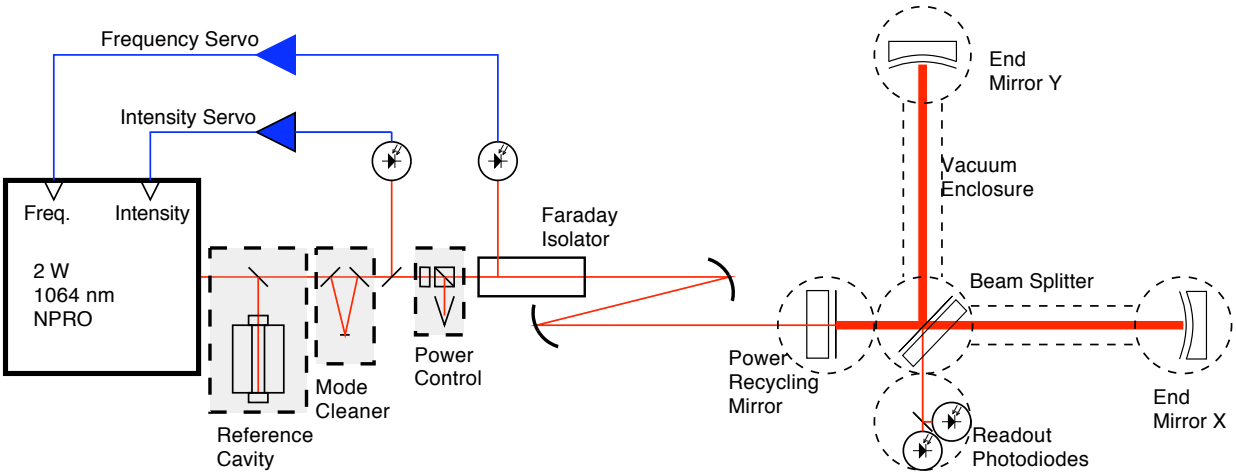

Figure 6: The holometer optical layout is based up a low noise Nd:YAG NPRO laser producing 2 W of 1,064 nm light. The light is intensity stabilized using a DC coupled photodiode, and the frequency is stabilized to the common mode arm length. The interferometer consists of a power recycling mirror, beam splitter, and end mirrors enclosed in an ultra high vacuum system. Although the readout photodiodes are shown enclosed in a vacuum system, initial commissioning will use in air photodiodes. The diagram also details the positions of optional subsystems – a fixed spacer reference cavity, laser mode cleaner, and power control – which will be installed as required.

noise in the transimpedance resistor, and voltage noise for the first amplifier.

Parameter	Value
Input Laser Power	0.75 W
Arm length BS-EM	40 m
Arm asymmetry (X-Y)	1 mm
PRC length PR-BS	0.5 m
End Mirror Transmission	10 ppm
Beam splitter Transmission	0.50
AR reflectivity	10 ppm
Mirror loss (PR, BS, EM)	50 ppm
Differential arm loss	25 ppm
Substrate loss	10 ppm
Transimpedance resistor	100 ohm
Voltage noise	3 nV/$\sqrt{\text{Hz}}$.

Table 1: Optickle simulation parameters used to estimate the $T_{\rm PRM}$ and δx.

The simulated interferometer operating parameters of $T_{\rm PRM} = 1,000$ ppm and $\delta x = 400$ pm, shown with a black diamond, are a compromise between phase noise sensitivity, $\phi(f) \sim 8 \times 10^{-12}$ rad/$\sqrt{\text{Hz}}$, and tolerance for each mirrors specific values of loss and absorption. With the slightly over-coupled configuration shown here, the cavity will remain over-coupled even if the loss is higher than predicted. Equally important, the power on the beam splitter

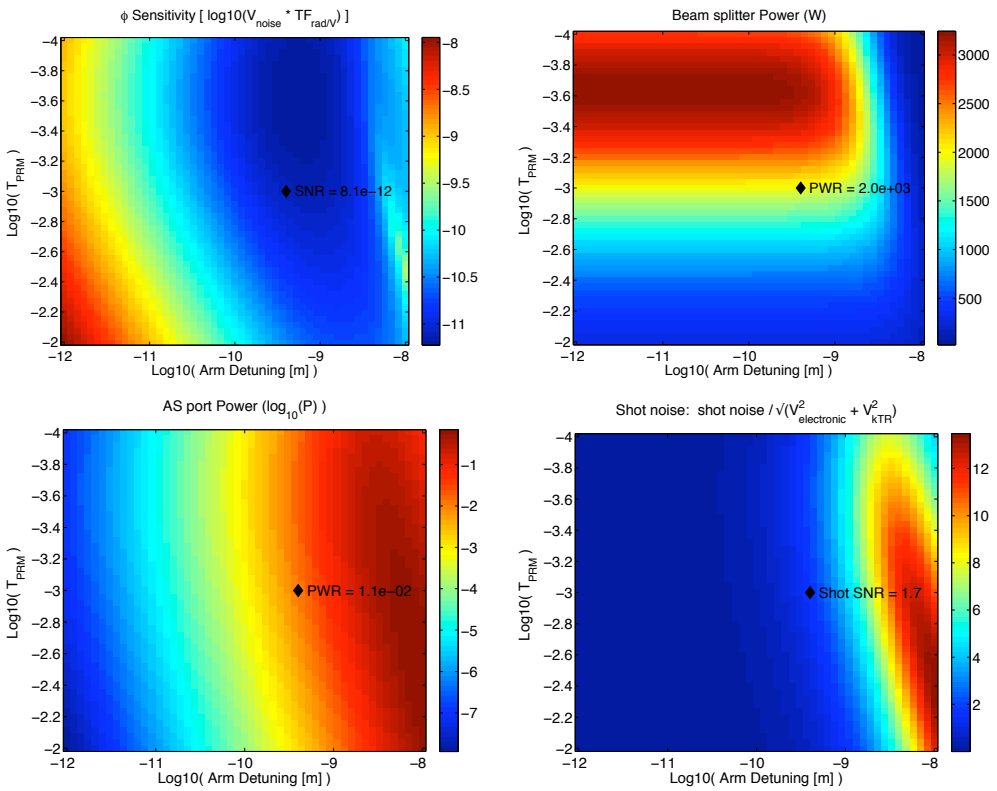

Figure 7: Interferometer parameters as a function of the power recycling mirror transmission (y axis) and the arm cavity offset (x axis). The noise limited phase contours show the interferometer differential phase sensitivity assuming shot noise, electronics noise, and Johnson thermal noise of the transimpedance resistor are the limiting noise sources. The black diamond indicates a good operating point with $T_{PRM} = 1,000$ ppm, and $\delta x = 400$ pm. For these settings the phase noise sensitivity is 8.1×10^{-12} radians/$\sqrt{\text{Hz}}$, the beam splitter power is 2 kW, the AS port power is 11 mW and the shot noise signal is 1.8 times larger than the dark noise.

and output photodiodes is manageable, if not exactly comfortable. The 2 kW of beam splitter power is larger than the LIGO interferometers, and somewhat less than the 5 kW used by GEO. The 5 mW per photodiode can be managed with modifications to the diode's DC gain described below.

C.2 Interferometer response

The interferometer frequency response, has also been modeled in Optickle for a realistic configuration with imperfect optics and arm lengths. The arms are modeled with a loss asymmetry of 25 ppm and a length asymmetry of 1 mm. At the operating point, the interferometer has a finesse of 6,200 and a corresponding cavity pole of 365 Hz. The transfer functions shown in Fig. 8 depict the length degrees of freedom to the respective sensors, including the cross terms. Of particular interest are the DARM to DC readout transfer function, showing a flat amplitude response with a phase delay, and the CARM to REFL_I signal showing the cavity pole. The two phases of the reflection error signal, REFL_I and REFL_Q, denote the In-phase and Quadrature-phase components of the RF demodulation

in the PDH detection. The RF phase has been set so that the CARM error signal is in the In-phase quadrature by convention.

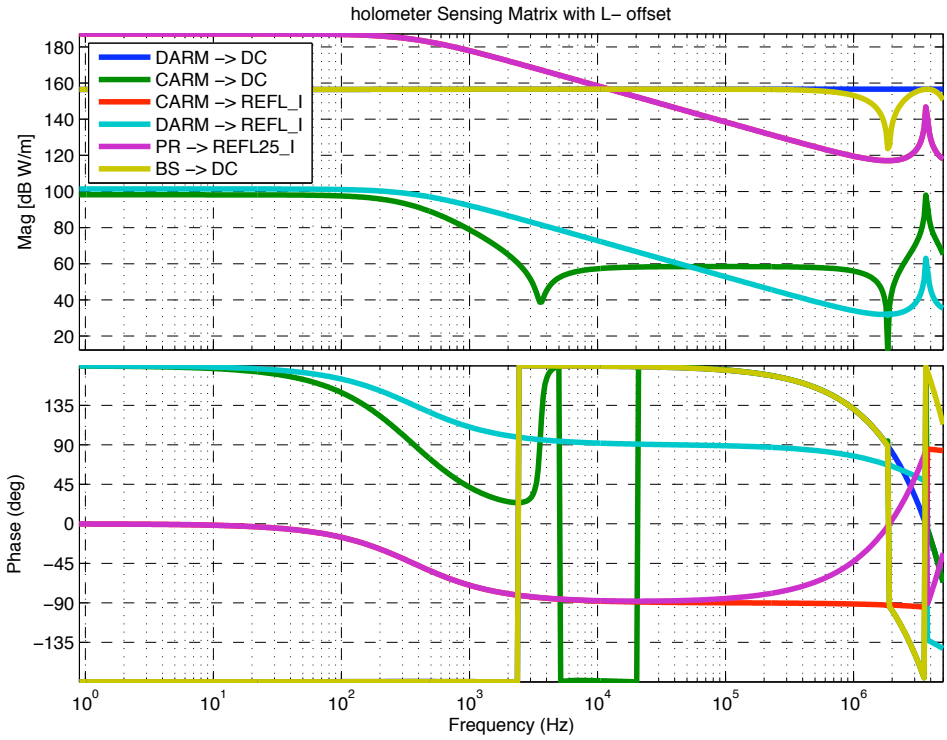

Figure 8: Transfer functions of the Holometer degrees of freedom to the sensing ports. The CARM and PR transfer functions to REFL_I are identical in magnitude and differ by a delay in phase. The DARM and BS degrees of freedom are flat, while the CARM DOFs have a cavity pole at 365 Hz, corresponding to a finesse of 6,000.

The cross terms in Fig. 8 will determine the performance requirements of the CARM servo loop and the laser frequency and intensity noise servos. For instance, the Michelson topology suppresses the CARM contribution to DARM by 90 dB at 100 kHz. From the cavity pole at 365 Hz to 3.5 kHz, the CARM signal couples to DARM via the DARM offset with a $1/f^2$ dependence. Above 3.5 kHz, the coupling arises from the macroscopic arm length asymmetry of 1 mm. Obviously, the CARM servo requirements are coupled to overall requirements on the interferometer configuration. A full noise budget analysis is required to specify the frequency, intensity, and DARM servos.

C.3 Lock acquisition

The very high interferometer finesse presents difficulties for lock acquisition because the CARM error signal is only linear over a few tenths of a picometer range, a fraction of the cavity bandwidth. Fortunately, the DARM offset controls the effective transmission of the Michelson, thereby controlling the interferometer finesse. The CARM fringe and the RF error signal are shown in Figure 9 for a variety of DARM offsets. As the offset is varied from the operating point at 0.4 nm to an offset of 16 nm the interferometer finesse varies from 6,000 to 600, easing the lock acquisition process.

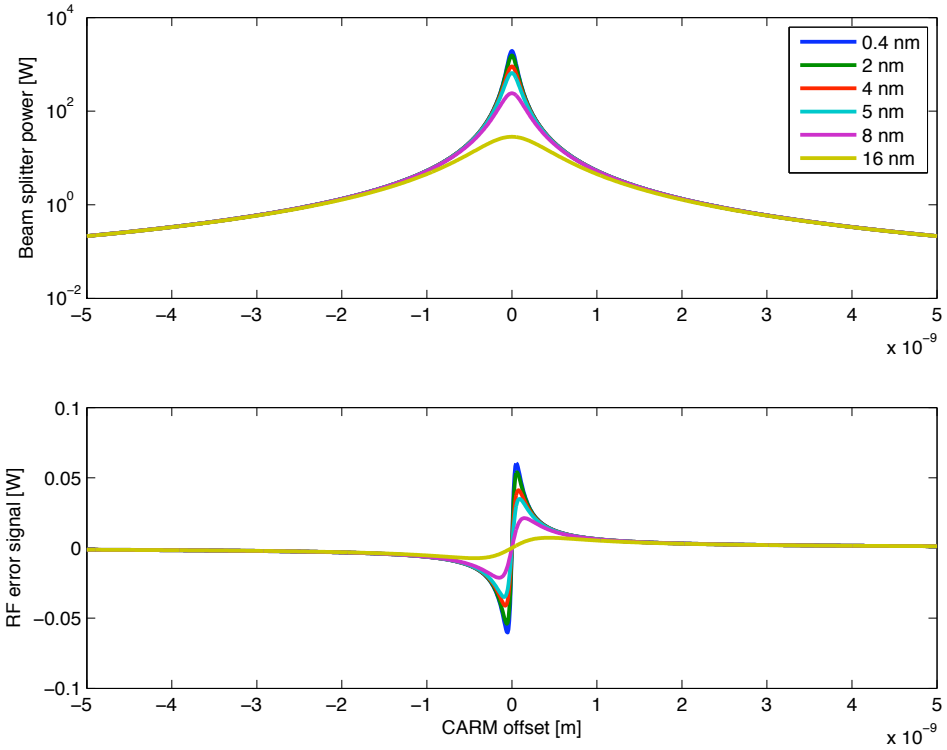

Figure 9: The CARM fringe as a function of the DARM offset for variable finesse locking. The CARM fringe finesse varies from 6,000 for the 0.4 nm offset to 600 for the 16 nm offset. This feature will be used during lock acquisition.

There are several difficulties associated with variable finesse locking that must be considered. First, the changing finesse shifts the cavity pole from 365 Hz at the operating point up to 3.5 kHz for the largest offset as shown in Figure. 10. Consequently the CARM servo must either have a very high bandwidth, a very low bandwidth, or compensate for the moving pole as the interferometer is brought into resonance. Second, the optical gain for the CARM degree of freedom decreases by the square of the change in finesse and may become electronics noise limited at large offsets, saturating the CARM actuation. Finally, as shown in Fig. 7 the power on the AS photodiodes may exceed 0.5 W as the interferometer sweeps through critical coupling. The AS photodiodes will have to be protected with a shutter and the DARM DC signal sensed with a high-gain, low-power photodiode during lock acquisition.

C.4 Laser

A Nd:YAG, Non-Planar Ring Oscillator (NPRO) is the interferometer's input laser. Lasing at 1.064 μm, the Nd:YAG NPRO has been used extensively in the gravitational wave and precision measurement fields because of its inherent low noise (few kHz free running linewidth) and extremely high reliability (several NPRO's used in LIGO have operated continuously for more than a decade). Commercially available NPRO's range in power from 0.5 W to 2.0 W. More costly Master-Oscillator, Power Amplifier lasers using an NPRO seed laser are available up to 35 W. The Optickle simulation above uses 0.75 W of input power; given normal optical losses a 1.0 W or greater NPRO is necessary.

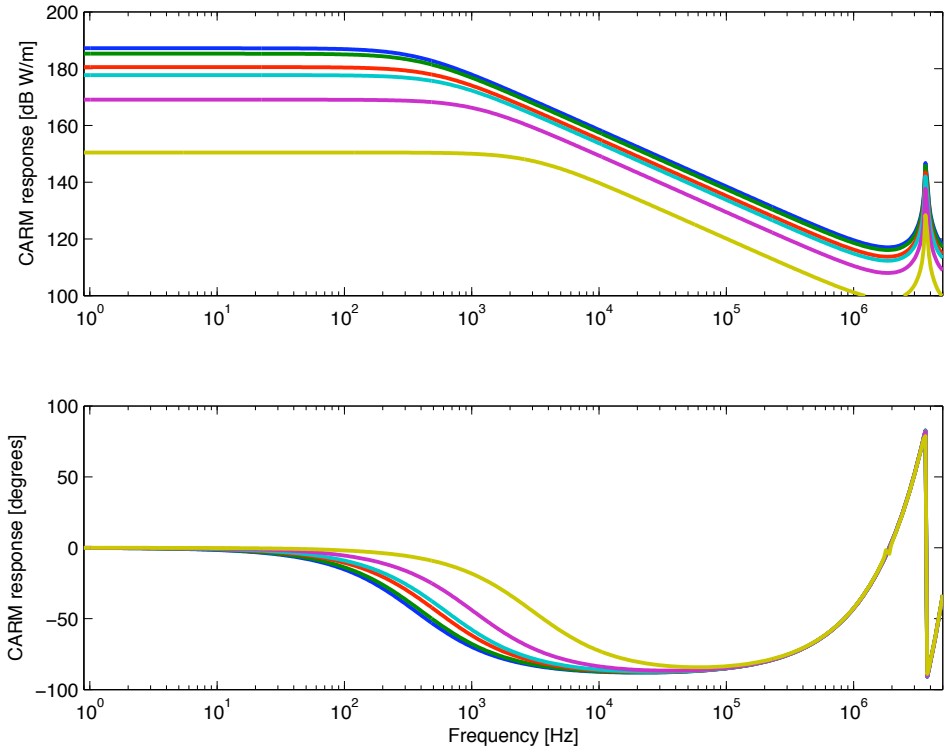

Figure 10: As the DARM offset decreases, the Finesse increases and the cavity pole moves from 3.1 kHz for the 16 nm detuning to 365 Hz for the nominal 0.4 nm detuning. The optical gain increases from 150 to 190 dB W/m over the same span. The CARM servo will have to compensate accordingly.

Although there are decades of experience using NPRO's in low noise interferometers, those instruments are low frequency devices whose low noise band extends to 10 kHz. Of particular concern is the frequency and intensity noise at the laser's relaxation oscillation frequency, 60-70 kHz, which lies outside the band of most current instruments. Furthermore, the laser in a gravitational wave detector or other precision experiment is filtered and stabilized with high finesse cavities to achieve shot noise limited performance. Consequently, the intensity and frequency noise characteristics of an NPRO in the holometer band from 10 kHz to 4 MHz are somewhat uncertain. Note that the differential readout of the Michelson interferometer is immune to laser noise to first order, however there may be excess coupling from imperfections. To deal with excessively high laser noise, the optical design in Figure 6 includes provision for an optional Frequency Stabilization Servo (FSS) and a Pre Mode Cleaner (PMC). The former stabilizes the NPRO to a fixed spacer, high-finesse reference cavity with a high bandwidth servo, while the latter provides passive filtering of laser noise using a high-finesse cavity.

C.5 Detectors

Commercial Thor Labs PD255 photodetectors have been modified for the holometer experiment to have a gain close to 1/2 at low frequencies and about 50 above 100kHz when loaded with 50 ohms. The schematic diagram is shown in Figure 11. The transfer function of the detector has been measured with an AM laser light source and referenced to a fast New Focus photodetector. The transfer function of two detectors are shown in the left panel of

Figure 12. The input voltage noise is approximately 3 nV/$\sqrt{Hz}$ with an input resistance of 100 ohms. The shot noise from 2.8 milliamperes of photocurrent equals the input noise of the preamplifier. The shot noise as a function of intensity at a variety of frequencies between 1 to 30 MHz has been measured with an Incandescent light source illuminating the detector through a low pass optical filter. The filter is opaque at wavelengths shorter than 8500A. The right panel of Figure 12 shows the results of these measurements. The noise exhibits the expected dependence but the absolute value is about 15% smaller than expected, possibly indicating some space charge storage in the detector. The detectors satisfy the requirements for the proposed holometer noise experiment for the initial phase where the detectors are placed outside the vacuum.

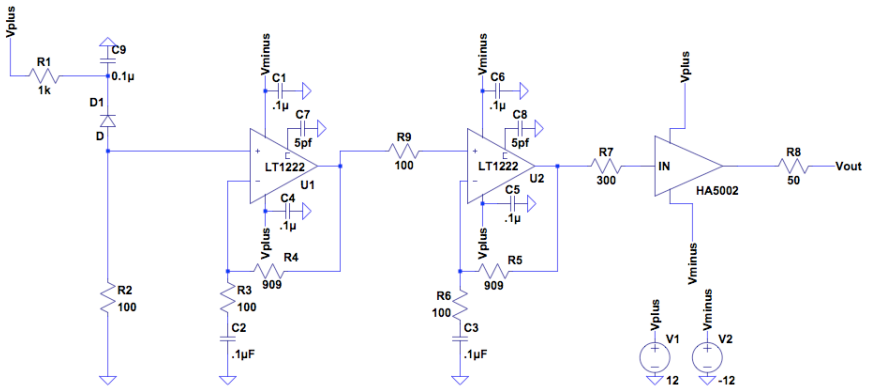

Figure 11: The schematic diagram of the modified PD255 photopreamplifiers. The modification consists of placing the 0.1 mfd capacitor in series with the 100 ohm resistors in the feedback paths of the LT1222 operational amplifiers. The capacitor limits the DC gain to 1/2 while keeping the gain above 100kHz at 50 when the amplifier is loaded with 50 ohms.

C.6 Noise Sources

Thermal noise in the transimpedance resistor and preamplifier noise Assume that we will be using RF components standard 50 ohm terminations. The thermal noise current generated by a 50 ohm resistor at 300 K is 2×10^{-11} amp/$\sqrt{\text{Hz}}$ and decent amplifier input noise is 1×10^{-9} V/$\sqrt{\text{Hz}}$. The Poisson noise of the modulated light should exceed these values by at least a factor of 3. The photocurrent that can be modulated needs to be 3 milliamperes or larger. With InGaAS photodiodes that have a quantum efficiency of 0.8, the power hitting the photodetector should then be about 4milliwatts/photodiode. With two photodiodes the antisymmetric power needs to be 8 milliwatts. These back-of-the-envelope numbers agree well with the more realistic Optickle simulation results above.

Poisson noise due to M1 M2 reflectivity unbalance The power at the antisymmetric output is second order dependent on the fractional difference in reflectivities of M1 and M2. The antisymmetric power varies as $\frac{P_{\text{in}}(\Delta R)^2}{2A}$. The reflectivities should be matched to 2×10^{-3} in order to minimize the shot noise from the resulting contrast defect.

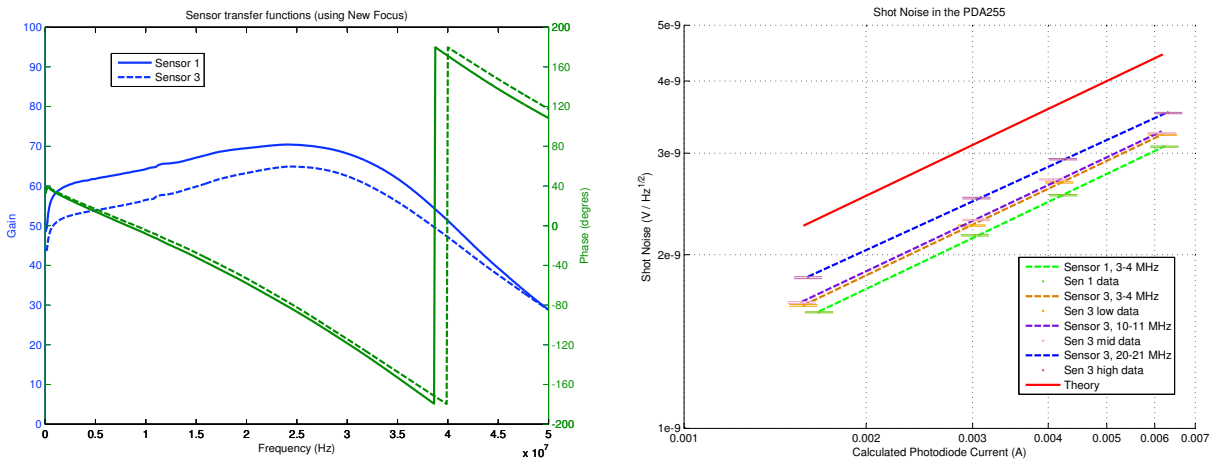

Figure 12: **Left:** The optical transfer function of the modified detectors. The detector is illuminated by an infrared laser AM modulated up to 70 MHz. The laser drive system has some frequency dependence so that a reference spectrum was taken with a fast 0.25mm New Focus photodetector to normalize the transfer function. The critical aspect for the holographic noise experiment is the smooth and slowly varying phase response which assures reliable cross correlation between the interferometers in the MHz band. **Right:** Shot noise measured from an incandescent source observed through a low pass optical filter. Points were taken at a variety of frequencies between 1 to 40 MHz and at several photocurrents.The square root dependence with input light power is obeyed but the absolute value of the shot noise is about 15% smaller than expected. The deviation could arise from space charge in the photodiode. Data taken and plotted by David Kelley.

Poisson noise due to rms relative motion of the mirrors M1 and M2. The relative motion of the two end mirrors should be smaller than the fringe offset determined by the amplifier noise. If one allows the relative motion to be equal to the offset, it corresponds to about 400 pm rms motion. If the relative vibrational noise in the space is 4 microns rms with most of the energy at 10 Hz and smaller, the feedback loop gain of the fringe control signal needs to be about 10^4 with a bandwidth of at least 10 kHz. The design of this servo with appropriate PZT controllers is one of main design tasks for the experiment once the vibration has been measured. There may be resonances in the structure which will require special filtering in the control system. There may also be pleasant cancellations due to common mode motion in the building. All this argues for a digital control system with the simplicity of digital filtering to control the feedback.

Equivalent phase noise from amplitude fluctuations The excess amplitude noise in the light above the Poisson fluctuations needs to be controlled to a level equal or below the Poisson noise. The Poisson fluctuations of the 4 milliamperes per photodiode corresponds to a relative intensity noise of 9×10^{-9}. The holometer signal band will be above 10 kHz so that the standard noise sources due to vibration and acoustic coupling will not be important. The relative intensity noise of a commercial NPRO was measured at LIGO and also in Hanover. At frequencies above 10 kHz one can achieve 10^{-7} with pump stabilization of the laser and 8×10^{-9} with external photodiode stabilization using electro-optic amplitude modulators. Alternatively or in addition

one can use an optical filter cavity which passively filters the intensity noise. High frequency amplitude noise does need to be tended to in this experiment, especially if there is a large contrast defect due to optic imperfections.

Direct phase noise from frequency noise The principal means for laser frequency fluctuations to cause phase noise in the interferometer is through path length difference between the two arms. In a Michelson interferometer it is reasonably easy to find the operating point that greatly reduces this source of phase noise . One executes a search for the "white" light fringe, the fringe that minimizes the modulation measured from a frequency modulated light source. The frequency noise of the laser filtered by the power recycling cavity should be less than $\nu(f) = 10^{-2}$ Hz/$\sqrt{\text{Hz}}$ above 10 kHz. The frequency noise sensitivity of the measurement is given by $\phi(f) = 2\pi\nu(f)\Delta x/c$. where Δx is the path length difference. The phase noise should be less than the Poisson driven phase noise given previously which requires the path length difference be less than 6 cm.

Phase noise from scattering paths For a critically coupled power recycled interferometer, the input laser power leaves the interferometer by absorption or scattering. When using low absorption mirrors, the entire input beam will be scattered out of the cavity. The noise generating, recombined scattering paths will typically involve scattering from a mirror, a reflection or another scattering by the wall, and ultimately recombination with the main beam on a mirror. We studied this process for LIGO in a model where the ground noise and acoustic excitation of the scattering surfaces phase modulate the scattering paths. To reduce multiple bounce scattering paths from mirror to mirror, LIGO baffles the tubes. At the frequencies involved in the holographic noise search the acoustic and seismic motions will not have components in the fringe interrogation band and even the worst case fringe wrapping motions are not expected to up-convert from the seismic and acoustic bands into the region above 10 kHz. Instead, the primary source of phase noise from scattering will come from the scattered beams having taken different paths than the main beam before recombination so that the scattered paths are not on a white light fringe. The phase noise is similar to the path length unbalance formulation above but with the ratio of the scattered field to the main field as an additional multiplying factor. The phase noise is

$$\phi(f) = \frac{2\pi}{c}\frac{\nu(f)}{|1 + if/f_c|}\Sigma_i\left(\frac{E_i\Delta x_i}{E_{\text{main}}}\right) \tag{16}$$

although this is a vector sum. Assume the longest scattering path is 40 m. Using the same NPRO frequency noise as above, filtered by the recycling cavity pole f_c, requires a scattered field to main field ratio of 10^{-4} or smaller at 10 kHz; an intensity ratio 10^{-8}. The LIGO experience is better than this requirement, however, there are specific locations where the scattered light is close to being specularly reflected where LIGO has had to erect blocks and baffles. Some care will need to be taken to reduce scattering from the beam tubes and from normal incidence surfaces in the vacuum system.

Phase noise from forward scattering by the residual gas Changes in the column density of the gas due to molecular motion causes fluctuations in phase from forward

scattering off the residual gas molecules. The scattered field by the molecules when recombined with the main beam causes the phase fluctuations (another way of talking about the index of refraction). The phase fluctuations from statistical mechanics are given by

$$\phi(f) = \frac{8\pi^2 \alpha L^{1/4} \sqrt{\rho}}{\lambda^{5/4} \sqrt{v}} e^{-\frac{f\sqrt{2\pi\lambda L}}{v}} \tag{17}$$

where ρ is the particle density in number/cc, α is the molecular polarizability in cc at the wavelength of the light and v is the molecular average velocity. The exponential reflects the fact that the distribution of molecules over the laser beam does not change faster than the time for an atom to cross the beam. Using $\alpha = 1.5 \times 10^{-24}$ cc as the polarizability of molecular nitrogen, and $v = 5 \times 10^4$ cm/sec as the thermal velocity of the molecule, the particle density to reduce this noise to 1/10 of the Poisson phase noise becomes 1×10^{13} molecules/cc or a pressure of about 10^{-4} torr. A more strict requirement on the vacuum pressure and in vacuum materials is to achieve 10^{-6} torr to avoid mirror contamination.

C.7 Development Efforts

The possible need for development of mirror mount actuators will depend on the seismic conditions at the chosen experimental site. Various seismic measurements have been performed at Fermilab in the past for accelerator projects. A sample power spectral density of vertical displacement is shown in Figure 13 using data taken at the E4R experimental hall at Fermilab, and published in Baklakov et al. (1999). According to LIGO experience, displacement noise of up to 1μm rms can easily be compensated using standard mirror actuators. More recent measurements performed at E4R and at nearby candidate site warehouses using magnetic seismometers confirm the generally low noise levels in the area. However, as bidding/procurement for warehouse leases commences, we will need to work with the DOE site office in assessing the seismic properties of candidate sites. If seismic levels at all candidate sites exceed the tolerance level for conventional actuators, then some development work will be needed to either mechanically dampen the seismic noise, or to develop actuators with larger dynamic range.

C.8 Cost

The power recycled interferometer requires low loss optics. Each interferometer has two end mirrors, one beam splitter, and one power recycling mirror. Each of these is on a piezo-controlled mount, costing $3k each. The optics need to be super polished, and coated with Ion Beam Sputtering (IBS). We know of 4 shops that do this: Research Electro-Optics, Coastline Optics, Gooch and Housego, and Advanced Thin Films. LIGO did a run with R.E.O. two years ago at a cost of $10k per coating run, $1k per substrate, with a 9-week lead time. We will need three coating runs (one for each of the three types of mirrors) and will coat extra mirrors in each run so we have spares on hand. We tabulate these costs in Table 2

As shown in Figure 6, the laser table holds the laser, systems to control the beam, and steer

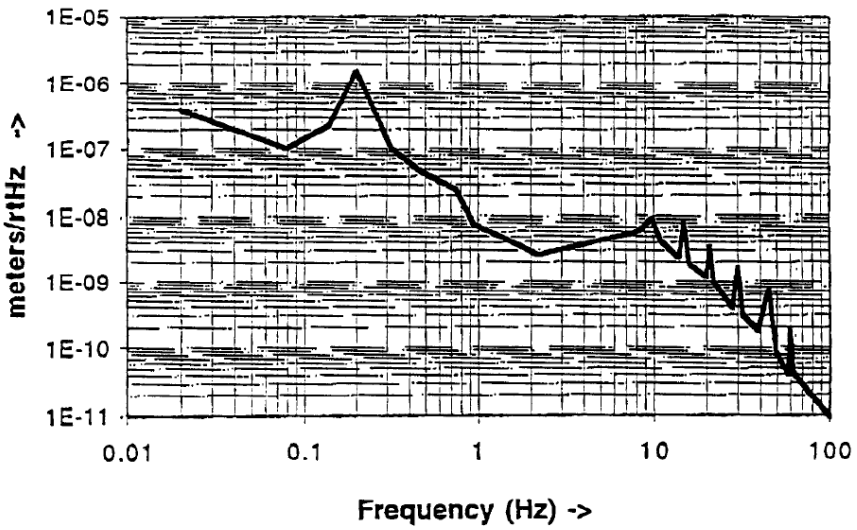

Figure 13: Power spectral density of vertical displacement seismic noise measured at the E4R building at Fermilab Baklakov et al. (1999). If noise levels at the chosen experimental site can be kept below 1μm rms as indicated here, the resulting phase noise in the interferometers can removed using feedback loops involving conventional mirror position actuators.

Item	No.	cost
End Mirror	6	\$16k
Power Recycling Mirror	4	\$14k
Beam Splitter	4	\$14k
Mounts	8	\$24k
Interferometer Optics Total		\$68k

Table 2: Costs for optics and mounts for the interferometers.

it into the interferometer. We tabulate the cost of each subsystem, based on the number of components, in Table C.8.

Subsystem	cost
Laser	\$60k
Reference Cavity	\$30k
Mode Cleaner	\$30k
Power Controller	\$5k
Detectors (incl. optics)	\$10k
Steering	\$5k
Total cost per Interferometer	\$140k
Laser Table Optics Total	\$280k

Table 3: Costs for optics and mounts for the interferometers.

D Electronics

As shown in Figures 3 and 8 and discussed in Section C.2, the signal is a power variation at the antisymmetric port from DC to about 4 MHz. At low frequencies, below 20 KHz, the positions of the end masses of the interferometer are servoed to maintain the system at a constant preset DARM in spite of of low frequency vibrations with amplitude that would exceed the linear range of the interferometer. Low frequency influences including seismic noise, thermal noise, acoustic noise, gas pressure fluctuations and thermal expansion among others. The end mirrors are controlled with piezoelectric positioners driven by the antisymmetric port output.

At high frequencies, above the DARM servo bandwidth, where the noise sources are those outlined in Section C.6, the system is open-loop. The high-frequency signal which is captured, and analyzed for the holographic noise correlation between the two interferometers. The two interferometer data taking systems will synchronize to absolute time derived from a GPS receiver and synchronized to each other using IRIG-B. Most of the electronics are contained in a PXIe chassis which contains the digital control loops, timing, and fast data acquisition and temporary storage. In addition to the PXIe chassis, near each of the three stations of the vacuum stations, a remote electronic enclosure containing a gain-setable buffer amplifier and analog Nyquist filter will provide the cable distribution for the vacuum station. Table 4 lists the main electronic components of the system.

D.1 Low Frequency Control Systems

The low frequency control system consists of a set of digital control loops, The loops have gain-settable preamplifiers and analog Nyquist filters following the photodiode preamplifiers shown in Figure 11 for each photodiode. The output of the digital loop filters are also buffered by remote analog output filtering circuits and control the piezoelectric actuators using commercial piezo-amplifiers. Gain and parameter setting in the preamplifier is accomplished with simple digital control of switches in the preamplifier circuit controlled by the PXIe chassis.

The digital filters themselves are implemented using National Instruments analog R-series I/O cards with onboard FPGA digital signal processing circuits. The boards are in a PXIe backplane chassis with a local control computer. The control loop filters are designed using simulation packages and a LabVIEW FPGA module specifically designed to implement digital signal processing on the R-series FPGAs. The filters can be modified in real-time from the control computer to implement the lock acquisition outlined in Section C.3.

The low frequency cards will generate housekeeping signals filtered to 100 Hz bandwidth for all sensor and drive signals. These signals are stored to disk for all times when the interferometer is running. If needed for diagnostics, full bandwidth servo information can also be stored.

#	Mfr.	Part No.	Item	Each (K$)	Total (K$)
2	NI	PXIe-1075	18-Slot 3U PXI Express Chassis	5.6	11.2
2	NI	PXIe-8106	Dual Core Controller (Windows XP)	4.2	8.4
2	NI		Additional RAM and System Disk, Screen, Keyboard	1.0	2.0
2	NI	PXIe-6672	Timing and Synchronization Module with TCXO	1.8	3.6
8	NI	PXI-7852R	LX50 Multifunction RIO (8 AI, 8 AO, 96 DIO)	3.8	30.4
4	NI	PXIe-5122	2-CH, 100 MS/s Digitizer w/8 MB/ch	5.8	23.2
2	NI	HDD-8264	12-Drive, 3 TB, 2U, Cabled PCIe RAID HDD Enclosure	5.6	11.2
2	NI		Sets of high density cables	1.8	3.6
2	NI		LabVIEW Development System and add on modules and drivers	6.9	13.8
2			Laser Intensity servo (locally built)	6.0	12.0
2	Vescent Photonics	D2-115	High-Speed Laser Servo	6.0	12.0
2			Preamps, Nyquist filter, and buffer amps, distribution circuits (locally built)	10.0	20.0
2			Piezo contoller systems	10.0	20.0
			DAC Sub Subtotal		107.4
			Intensity and Frequency Servos Subtotal		64.0
			Total Electronics		171.4

Table 4: Electronics Parts and Equipment Cost Estimate

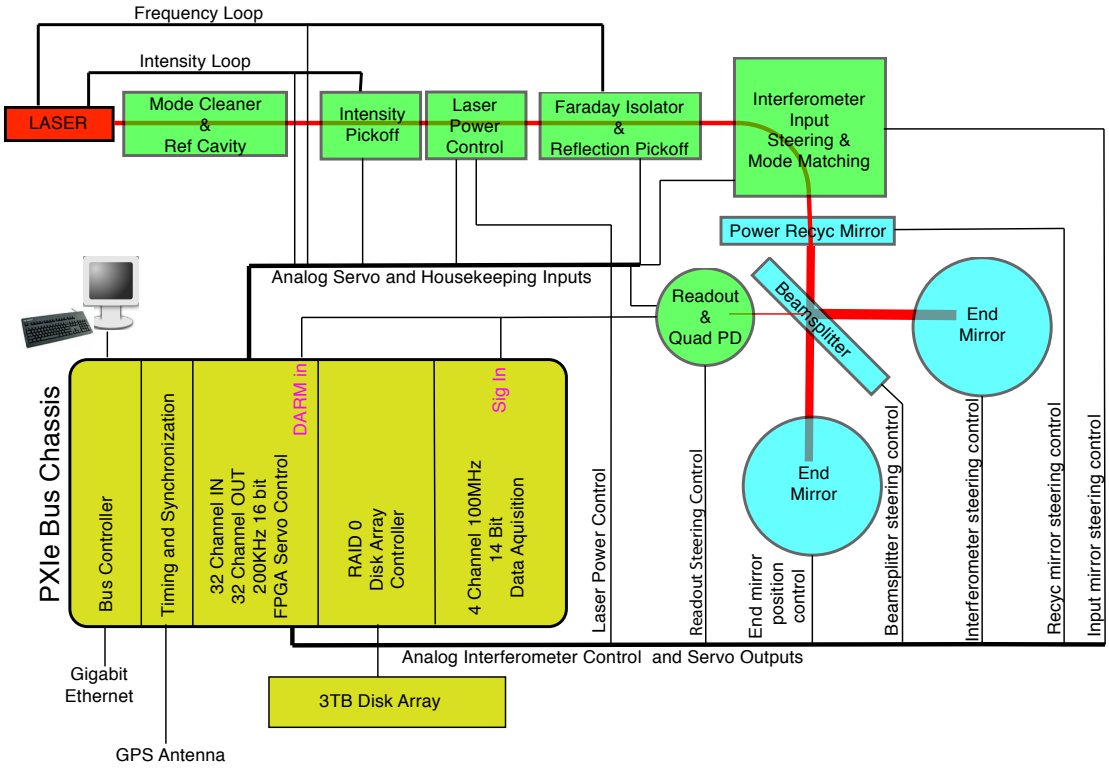

Figure 14: Schematic diagram of the electronics for each interferometer. Residing in a PXIe chassis are the low frequency control loops, implemented with digital filters, and the high-frequency data acquisition boards and data storage. Not shown are the remote buffer amps and Nyquist filters.

D.1.a Laser Frequency and Intensity Servos

The Nd:YAG NPRO laser intensity is stabilized using a DC coupled photodiode following a pick-off mirror located as shown in Figure 6. The bandwidth of the intensity servo is high enough and its design simple enough that it will be implemented in analog. The design of this circuit will follow that of the Advanced LIGO prototype which uses a similar laser.

The frequency of the laser is locked to the common mode interferometer arm length using PDH stabilization (Black, 2001). As shown in Figures 6 and 14, the servo error signal is obtained from the reflected light from the interferometer power recycling mirror and the Faraday Isolator. The laser is equipped with a frequency adjustment input which adjusts the laser cavity length with an internal PZT at high frequencies and a temperature control at low frequencies. The error signal is derived from a PDH locking system at the interferometer reflected port. The baseline plan is to control this loop using a commercially available laser stabilization unit.

D.2 High Frequency Signal Capture

The intensity of the radiation on the antisymmetric port of the interferometer is servoed to a preset level (and thus differential arm phase) by the low frequency differential arm loop. The loop bandwidth is about 10KHz and above that frequency the differential arm length degree

of freedom is not controlled. The signal extends from 10 KHz to the free spectral range of the interferometer, about 4MHz. The two readout diodes have a bandwidth of greater than 37 MHz as discussed in Section C.5 and shown on the left in Figure 12.

D.2.a ADC and Data Streaming

Each interferometer PXIe chassis will be equipped with two National Instruments fast data acquisition boards, each operating at 100 MHz maximum sample rate in two channels for a total of 4 channels per interferometer. The baseline plan is to have only two 20MHz streams from each interferometer but the remaining channels are designed for system diagnostics and debugging. The data will stream from the two boards to a 12 disk RAID-0 array. The ADC cards can stream directly to the disk array using the PCIe fast channels without intervention from the bus control computer. The initial arrays use 12 250GB disks but an upgrade to 500GB drives will enable 6TB of RAID 0 storage for each interferometer.

D.2.b Data Storage

The interferometer high-frequency signal for each interferometer is 80 MB/s. The low-frequency housekeeping is $<$ 30KB/s. To obtain a high signal-to-noise ratio on the holographic noise, 10 hours of integration is required. Thus 'run' for both interferometers generates about 6TB. Only a few such data sets will need to be stored long-term. After a run, data stored on the RAID disks will be unloaded using a gigabit ethernet to a lab computer. Lossless compression can reduce this by about a factor of 2. The data can be analysed into cross-correlation data sets with loss of original data but no loss of holographic noise information by generating the cross spectra with resolution of 10 KHz and highest frequency 10 MHz. If 10 such complete 4x4 cross spectra are accumulated per second the data rate is 1.2MB/s and a 10 hour run including housekeeping is 40 GB. A large number of runs can easily be stored in this form with almost no loss of information.

D.3 Training and Development Efforts

We continue to work in the Linac Laser Lab at Fermilab to train scientists in optics and control. We have successfully implemented Pound-Drever-Hall control of an optical cavity. We intend to purchase one DAC system so we can learn how to control mirrors and operate an optical cavity and a power recycled interferometer. We will also use this lab to test electronics for the intensity and frequency servos.

E Mechanical

The mechanical system of the holometer consists of the vacuum system and other required mechanical infrastructure to support the experiment.

E.1 Vacuum

E.1.a Overview of Requirements

The vacuum system for the holometer has the general requirement that it houses the optics of the interferometer in a manner that allows for the required optical performance to make the holographic noise measurement. Air currents or significant residual gas ($> 10^{-6}$ Torr) can cause instabilities and scattering in optical beams. Hydrocarbons and dirt/dust can reduce optical performance of mirrors, beam splitters, and other optical components. The vacuum system must suppress scattered light through baffles. The system must also allow for an interface to the laser and input optical beam, an interface to the detectors and data acquisition system, and interfaces to ancilliary sensors and other diagnostic, monitoring and safety equipment. In addition, the vacuum system must allow for optical alignment and the servicing of individual optical elements that make up the system. During data taking, the vacuum system cannot induce vibrations and cannot inject electrical noise that significantly degrades the optical performance. The requirements need to be met such that the vacuum system has limited impact on the overall scope of the project in terms of the required running time. For example, the pump down time of the interferometer or a chamber must not be so long that would require a substantially increased time period in which the the experiment is conducted. The proposed implementation of the vacuum system includes standard and semi-custom ultra-high vacuum components procured in a manner that lessens the need for Fermilab mechanical engineering and technical resources.

E.1.b Mechanical Implementation

A schematic of the proposed implementation is in Figure 15. Each of the two interferometers has a separate vacuum system consisting of two 40 m long arms that terminate into a service vessel which house the end mirrors. A central area has three service vessels: a middle vessel that houses the beam splitter, a vessel that houses the sensor, and a vessel that houses the interface from the input laser light and recycling mirror. All components are either off the shelf or are semi-custom in the sense that they are slightly modified from off the shelf parts. The majority of the components are composed of 304 stainless steel that will be delivered clean for ultra high vacuum use. The tubes themselves will consist of segments of 10 feet long 6 in diameter tubing which have 8 in outer diameter (OD) ConFlat-style (CF) flanges - one fixed and one rotatable. Each 40 m long arm will be composed of 12 such 10 ft long segments. Each arm will also include three standard tee's consisting of mating 8 in OD flanges and a standard 2 3/4 in CF port. These ports provide a means for additional pumping ports and for instrumentation and gauges within the arms. The arms will be separated from the service vessels first by means of an edge welded bellows and then by means of standard gate valves for the 6 in tubing. The gate valves function to preserve vacuum conditions inside the tubing in the event that the service vessels are opened for alignment or other activities. Each service vessel will be based upon a standard 24 in diameter vessel with four 8 in OD ports that interface with the arms or other vessels and two 2-3/4 in and two 3-3/8 in ports (eight ports for each service vessel) for connection to pumps, instrumentation/gauges, and a 2 in window for monitoring the system. The floor of each service vessel will have 1/4-20 blind tapped holes on 1 in centers for mounting optical components. The top of service

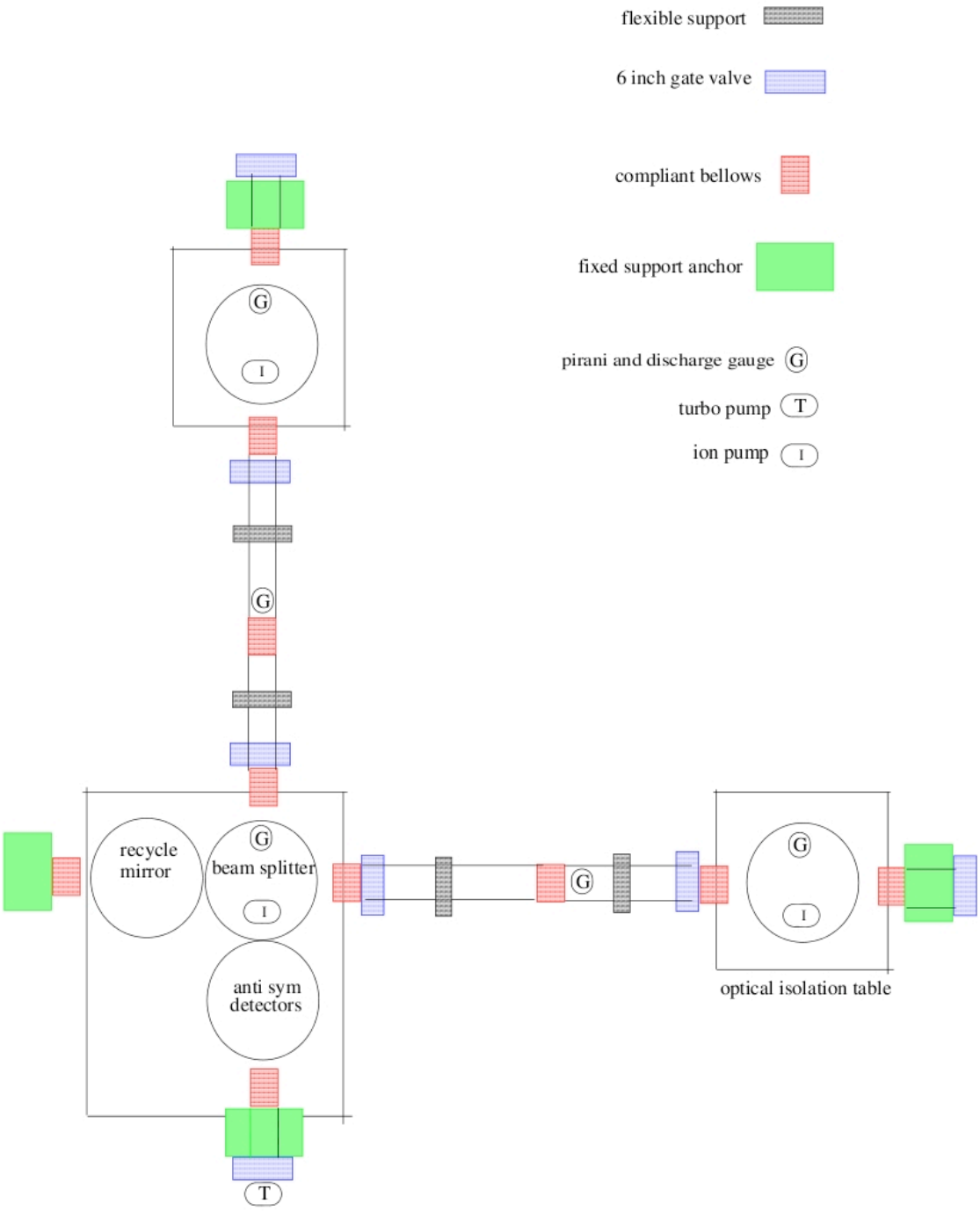

Figure 15: Schematic overview of one vacuum system. Please note that the components are not drawn to scale. Each of the round vacuum service vessels is 2 feet in diameter, the beam pipes are nominally 6 inches in diameter, and the arm length is 40 meters.

vessel will be a flat plate that could be a bell jar if additional vertical space is needed (in case, suspended optics is found to be required). The flanges around the service vessels will be outgassed Viton-type seals free of mold release and organic binders. The outer service vessels that hold the mirrors at the end of each arm will use a port to connect the vessel to a fixed support anchor so that no atmospheric pressure imbalance exists. The fixed support anchors will also attach to the service vessels that hold the laser and detector components. The service vessel holding the beam splitter will utilize all four of the 8 in OD ports.

A vacuum vending company has provided a detailed cost breakdown of the above system. With a 10 week delivery, the cost for the entire system for both interferometers amounts to approximately $250K. Details can be found in the Appendix on cost, schedules, and resources.

E.1.c Pumps

The vacuum pumping system allows for a pump down and hold at a level everywhere below 10^{-6} Torr. In order to not introduce hydrocarbons, oil free turbo backed by oil free scroll pumps provide the initial vacuum before ion pumps are turned on to achieve the final vacuum rates. This system allows the components that induce vibrations (turbo and scroll pumps) to be turned off while the ion pumps maintain high vacuum. The ion pumps are required to be baffled from emitting light and RF into the system.

A full engineering study of the pump down performance and optimization is not finished. However, a vacuum vendor has provided a first pass at such calculations using a system comprised of a single roughing oil free scroll pump (584 L/min) and a magnetically levitated turbo pump (1300 L/s). Ion pumps (100 L/s) are attached to the outer four service vessels. In order to achieve reasonable pump down times and to use standard gate valves, the plan is to bake the tubes and pump them down where much of the water has been driven from the steel. The tubes can then be closed off by the gate valves and the service vessels can be pumped down until the entire system is at a pressure when the gate valves to the tubes can be opened under vacuum. It is envisioned that two vacuum carts accomplish pump down of service vessels. The budgetary cost of the pumps from web sites is $10K for the scroll pump and $40K for the turbo pump with controller, This leads to a cost of $100K for the two vacuum pumping carts. There will be ion pumps on each service vessel. A total of 10 ion pumps (five for each interferometer) has a cost estimate of $25K including controllers. A grand total estimate for vacuum pumps is thus $125K.

E.1.d Gauges, Vacuum instrumentation, leak detector

Guages such as pirani and discharge gauges readback the the vacuum to verify it is maintained at required levels. These gauges along with additional vacuum pieces fall into an estimated miscellaneous $10K assigned to the vacuum system. Each vacuum system should have a residual gas analyzer ($5k each). We will also need one leak detector for diagnostics, with an approximate cost of $30K. A total for gauges, instrumentation, and leak detector, $50K.

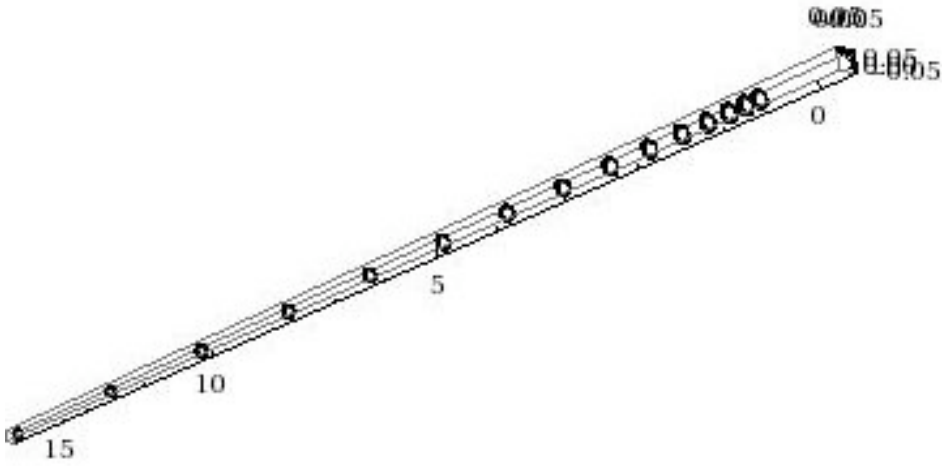

Figure 16: Side view of baffle locations in beam tube, showing one half of a beam tube. (Units are meters)

E.1.e Baffles

Light scattering from the walls of the vacuum chamber would contribute to unwanted noise in the interferometers. To reduce the effects of scattered light, a series of baffles will be inserted at geometric intervals along the length of each arm such that no portion of the walls are "visible" to the mirrors at either end, as shown Figure 16. An appropriate baffle may be constructed from a C-shaped piece of sheet metal that is bent into the proper shape (Figure 17) and then inserted into the vacuum pipes. The baffles will be held in place by friction. A simple tool can be designed to insert the baffles at desired location. Cost of the baffles and insertion tool is estimated to be \$10K.

E.2 Portable Clean Rooms

When the service vessels are opened for alignment or other activities, the area is to be kept clean so that dust and other contamination is reduced. This can be accomplished through the use of clean rooms. After moving the vacuum tubes in place, we need to simultaneously access the service modules near the beam splitter and the two service modules at the end mirrors. We will construct portable clean rooms and deploy them as needed.

A small clean room, 8' × 12' requires 4 blowers. We will use strip shields for the walls to simplify access for the vacuum tubes. Including two light fixtures, we estimate from prices on the Terra Universal prices that a small clean room will cost \$8K. Scaling by area, a large room is \$32K. We need one large and two small portable clean rooms, for a total of \$48k. Our plan is to access only one interferometer at a time, so they can share the portable clean rooms.

E.3 Laser and Optics Tables

Optical tables with off the shelf vibration isolation are required to support the laser system, central service vessel area, and separate tables to support the service vessel at the ends of

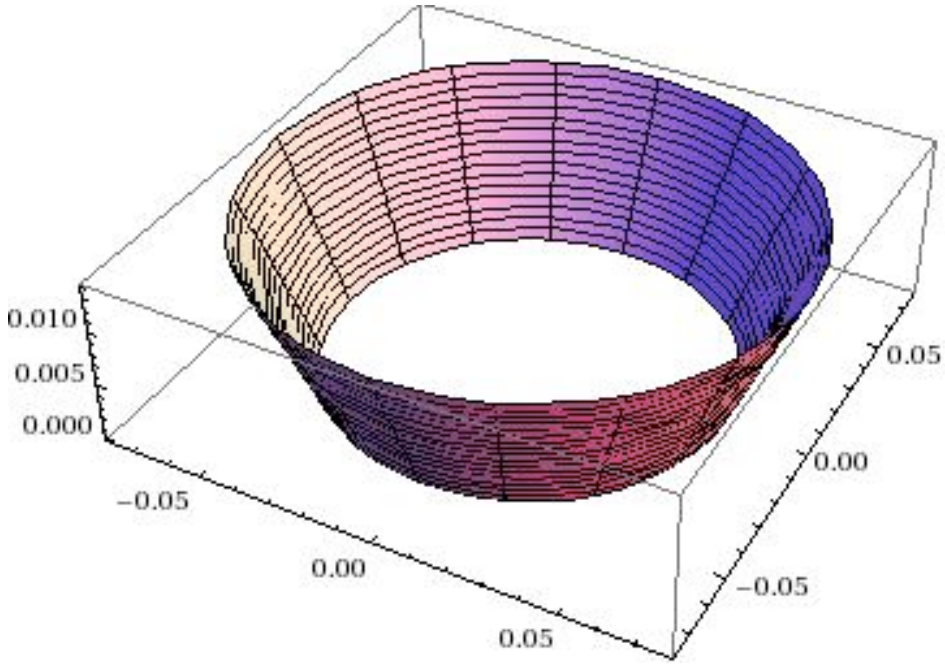

Figure 17: One baffle, which is to be inserted into the beam tubes. (Units are meters)

Item	qty	cost	line
Frame	1	$3,000	$3,000
HEPA	4	$700	$2,800
Light	2	$200	$400
Walls	40’	$40	$1,600
TOTAL			$7,800

Table 5: Cost for one small clean room

each arms that house the return mirrors. Each interferometer should be able to use four optical tables such as Newport ST Series with size 5 ft × 6 ft × 8 in ($7585 ea.) with CI-2000 Series vibration isolating legs ($4650 per table). An additional amount of $20K is added for pumps and other table accessories for a total estimate of $120K.

E.4 Support Stands

The support stands for the interferometer are expected to be simple stands constructed out of prefabricated flexible building material such as unistrut. The stands will allow for alignment of the vacuum system and will utilize pipe support with off the shelf vibration isolation. The stands will be bolted to the floor. An estimate of $400 per 10 ft long section of vacuum tubing yields a cost estimate of $16K for support stands.

Figure 18: One large version of the portable clean room and two small versions will be used while accessing the clean optics inside the vacuum service vessels. Laminar flow from the ceiling maintains a clean environment, once loose debris and dust is cleaned from the floor. Monitors inside each of the clean rooms will ensure that the system is working as expected after a move, before we open the vessel to access clean optics.

E.5 Infrastructure

We plan to rent commercial space near Fermilab. Our power and environmental requirements are met by spaces typically used for warehouse, light industrial, or retail. The cost scales with the size of the usable floor space.

Table E.5 summarizes the floor space (length and height) required for various configurations. The smallest possible area has dimensions $L \times L$ and allows us to measure correlations of 0% and 100%. Increasing the length of the building to $1.5L$ and $1.87L$ allows measurement of intermediate correlation strengths via rotation and translation, while a length of $2L$ allows measuring the coherence all the way down to 0% via translation and rotation. Increasing the size in the other direction allows us to measure the shape of the $\Xi(\tau)$. The largest space, $2L \times 2L$ allows all configurations.

The cost of a larger space needs to be balanced against the benefits.

Δ_X/L	Δ_Y/L	θ	length/L	height/L	area/L^2	$\Xi(\tau_0)/\Xi(\tau_0)_{max}$
0.00	0.00	0.0	1.00	1.00	1.00	1.00
1.00	1.00	180.0	1.00	1.00	1.00	0.00
0.50	0.00	0.0	1.50	1.00	1.50	0.50
0.00	0.00	30.0	1.50	1.00	1.50	0.87
0.25	0.25	0.0	1.25	1.25	1.56	0.75
0.00	0.00	45.0	1.71	1.00	1.71	0.71
0.00	0.00	60.0	1.87	1.00	1.87	0.50
0.00	0.00	90.0	2.00	1.00	2.00	0.00
1.00	0.00	0.0	2.00	1.00	2.00	0.00
1.00	1.00	0.0	2.00	2.00	4.00	0.00

Table 6: Usable Floor Space

F Cost, Schedule, and Resources

The project will proceed in three phases: design, construction, and operations. We are currently in the design phase. This effort has been continuing since the Spring of 2009. We had an informal review in the FCPA on June 9, 2009, followed by a presentation to the PAC in June, 2009. The design phase will continue after this PAC review in parallel on the optics, electronics, and mechanical subsystems. We plan to culminate this process with a final design review in February, 2010, before final authorization, ending the design phase and begining construction on March 1, 2010. This phase will consist of spending on order of $1M for purchasing vacuum, optics, and electronics from vendors. The duration of this phase depends on lead times for these items, which we expect to be less than three months. On June 1, we plan to begin the operations phase of this project when the components are all available "on the floor" of the warehouse.

The continued development and construction requires that some items be purchased before

the construction phase. We will use funds from the FRA grant of A. Chou and S. Meyer to purchase the LavView systems specified in this proposal in November, 2009. This will allow us to begin training in the use of this system to controlling and aligning optics in the current laboratory space we are using at Fermilab. A separate system will be installed at U. Chicago to characterize detector and readout noise.

We will also purchase some of the optical components required for the laser tables. We will use them in the existing linac laser lab at Fermilab to continue training of key personnel and development of control algorithms and software.

Obtaining a suitable operations space will be handled by the Chicago Office of the DOE. The Fermilab FESS studied options for constructing or modifying space on site and renting off site. Their conclusion is that it is more cost effective to rent commercial space near Fermilab, as modifying existing buildings at Fermilab or building a new site cost ∼$1M. We will work with the Department of Energy Chicago Office to specify the requirements, so that they can obtain a lease for space by June 1, 2010.

We plan to begin the operations phase of the project on June 1, 2010. After initial preparations described below, we will work in parallel to commission the laser tables and the vacuum systems. After installing the interferometer optics in the vacuum system, we can then operate the interferometers and measure their performance in place. Once both interferometers are working, we will begin the correlation measurments. One run to obtain significant signal/noise takes < 1 day. Moving one of the interferometers takes one or two days, so in principle all of the measurements could happen in two weeks. However, the challenge of this project is to demonstrate that we understand the systematic effects of correlated and uncorrelated noise from prosaic sources. The apparatus is designed with maximum flexibility with this goal in mind. We will move the interferometers and swap parts to study the systematics. Our conservative schedule calls for one year of commissioning and two years of operation. We will work with laboratory management during operations to refine this schedule.

F.1 Tasks

The experiment consists of the following systems. We use these categories to estimate cost, schedule, and resources for the design, construction, and operations phases.

Laser Table Optics optical components and mounts for the reference cavity, mode cleaner, power controller, faraday isolator, and mode-matching optics

Interferometer Optics power recycling mirror, end mirrors, and beam splitter, and mounts for the interferometers.

DAC System Hardware and software to control mirrors and read out detectors

Intensity and Frequency Servos analog feedback loop for laser intensity and frequency

Operations Space Compute Infrastructure networking, servers, printing, and security at the operations site

FNAL Compute Infrastructure data archiving and analysis at Fermilab

Vacuum Vessels and Tubes service vessels and the beam tubes

Vacuum Pumps and Instrumentation pumps, monitors, and residual gas analyzer

Support Stands for service vessels and vacuum system

Baffles Design the baffle layout and installation

Laser Table (mechanical) portable, stable table with acoustic baffling

Portable Clean Room to enclose service vessels while installing and adjusting optics

Safety movable partitions to isolate workspace while installing and adjusting optics, laser safety and vacuum safety equipment

Operations Space warehouse, retail, or light industrial space leased for operations phase

Task	Design ongoing until March, 2010	Construction March 2010 - June 2010
DAC System	purchase one system; 4 weeks lead time	purchase second system; 4 weeks lead time
Laser Table Optics	small table training and development; 12 weeks	purchase; 4 week lead time
Interferometer Optics	”	purchase; 10 week lead time
Intensity and Frequency Servos	”	
Operations Site Computing	requirements analysis and implementation plan; 2 weeks	purchase; 1 month lead time
Fermilab Computing	analyze disk/tape/robot optionss; 2 weeks	
Vacuum Vessels and Tubes	vet design; 8 weeks	purchase; 10 weeks lead time
Vacuum Pumps and Instrumentation	“	“
Support Stands	design; 2 weeks	fabricate; 8 week lead time
Baffles	design and prototype; 7 weeks	fabricate; 4 week lead time
Laser Table (mechanical)	design; 2 weeks	fabricate baffle; 4 week lead time
Portable Clean Room		purchase; 6 week lead time
Safety	review laser and vacuum design and operations plans; 1 week	
Warehouse	8 weeks specify	8 weeks bid and approve

Table 7: Duration of Tasks

Task	Design	Construction	Operations
DAC System	$54K	$54K	
Laser Table Optics	$140K	$140K	
Interferometer Optics		$68K	
Intensity and Frequency Servos	$32K	$32K	
Operations Site Computing		$40K	
Fermilab Computing			$70K for 70 TByte
Vacuum Vessels and Tubes		$250K	
Vacuum Pumps and Instrumentation		$175K	
Support Stands		$30K	
Baffles		$10K	
Laser Table (mechanical)		$120K	
Portable Clean Room		$48K (Terra Universal web)	
Safety		$10K (goggles, partitions, interlocks)	
Warehouse			$900K
TOTAL	$226K	$977K	$970K

Table 8: M&S Costs

F.2 Cost Roll Up

During this ongoing design phase we plan to spend $226k in M&S and $98k in non-scientist salary (fully-loaded). The construction M&S cost is $977k with $58k non-scientist salary. With a 50% contingency, the construction budget total is $1.55M. The total operations cost over three years is $970k M&S and $381k non-scientist salary. With a 50% contingency, the operation budget is $676k/year over three years.

Task	Design	Construction	Commissioning (6 months)	Measurement
DAC System				
Laser Table Optics	1.00 EP	1.00 EP	1.00 EP	
Interferometer Optics				
Optics Mounts				
Intensity and Frequency Servos	2.00 EE; 0.50 MT	4.00 ET	0.50 ET	
On Site Computing	0.25 CP		0.25 CP	
Off Site Computing	0.25 CP			
Vacuum Vessels and Tubes	0.25 ME		1.00 MT	continuing 0.25 FTE MT
Vacuum Pumps and Instrumentation	0.25 ME		1.00 MT	continuing 0.25 FTE MT
Support Stands	0.25 ME		1.00 MT	
Baffles	1.00 ME		1.00 MT	
Laser Table (mechanical)	0.25 ME		1.00 MT	
Portable Clean Room			1.00 MT	
Safety				
Warehouse				continuing 0.5 FTE MT
TOTAL non scientist FTE months	6.0	5.00	7.75	continuing 1.0
Cost w/OPTO/vac/fringe/overhead	$98k	$58k	$84k	$297k

Table 9: FTE months non scientist effort: CP=computing professional; MT=mechanical tech; EE=Electronics Engineer; ET=Electronics tech; ME=mechanical engineer; EP=engineering physicist. The FTE cost uses PPD rates for FY2009 inflated by 3%, with OPTO, vacation, fringe, and overhead included.

References

B. Baklakov et al. Ground motion measurements for Fermilab future collider projects. *Prepared for IEEE Particle Accelerator Conference (PAC 99)*, 1999. Prepared for IEEE Particle Accelerator Conference (PAC 99), New York, New York, 29 Mar - 2 Apr 1999.

E. D. Black. An introduction to pound–drever–hall laser frequency stabilization. *American Journal of Physics*, 69(1):79–87, 2001. doi: 10.1119/1.1286663.

C. J. Hogan. Measurement of quantum fluctuations in geometry. *Phys. Rev. D*, 77(10): 104031–+, May 2008a. doi: 10.1103/PhysRevD.77.104031.

C. J. Hogan. Indeterminacy of holographic quantum geometry. *Phys. Rev. D*, 78(8):087501–+, Oct. 2008b. doi: 10.1103/PhysRevD.78.087501.

C. J. Hogan. Holographic Noise in Interferometers. *ArXiv e-prints*, 0905.4803, May 2009.

C. J. Hogan and M. G. Jackson. Holographic geometry and noise in matrix theory. *Phys. Rev. D*, 79(12):124009–+, June 2009. doi: 10.1103/PhysRevD.79.124009.

D. Shoemaker, R. Schilling, L. Schnupp, W. Winkler, K. Maischberger, and A. Rüdiger. Noise behavior of the Garching 30-meter prototype gravitational-wave detector. *Phys. Rev. D*, 38:423–432, July 1988. doi: 10.1103/PhysRevD.38.423.

M. E. Zucker. The LIGO 40 m prototype laser interferometer gravitational wave detector. In *Marcel Grossmann Meeting on General Relativity*, pages 224–226, 1992.

G Appendix: Gaussian beams

The expansion of the transverse radial size of a Gaussian beam of wavelength λ upon propagation over a distance z from its waist position is given by

$$w(z) = w_0\sqrt{1+\left(\frac{z}{z_R}\right)^2} \tag{18}$$

where w_0 is the waist radius, defined implicitly in the 2-dimensional Gaussian intensity profile in radius r:

$$I(r) = I_0 e^{\frac{-2r^2}{w_0^2}} \tag{19}$$

and z_R is the Rayleigh range

$$z_R = \frac{\pi w_0^2}{\lambda}. \tag{20}$$

Eq. 19 is the conventional definition of the beam waist as the $1/e$ radius in electric field, corresponding to the $1/e^2$ radius in photon intensity. By comparing Eq. 19 to a conventional Gaussian function

$$I(r) = I_0 e^{\frac{-r^2}{2\sigma_0^2}} \tag{21}$$

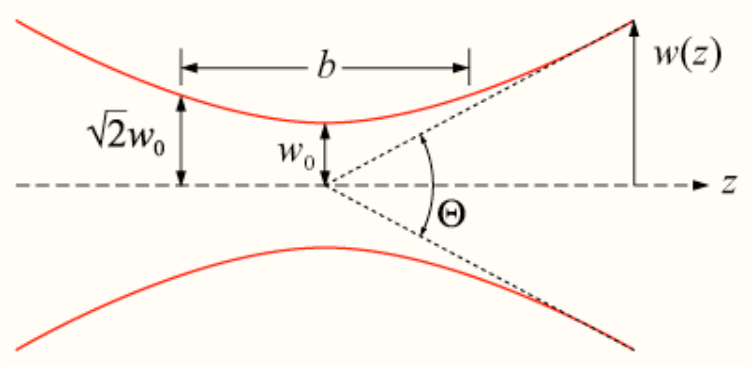

Figure 19: Due to the Heisenberg uncertainty principle, a beam of wavelength λ which is localized in transverse position to a precision $\sigma_0 = w_0/2$ will subsequently diverge with divergence half-angle $\theta = \Delta p_t/p = \lambda/(4\pi\sigma_0)$. While this diffraction angle is tiny for wavelength $\lambda_p = 1/M_p$, the effects can be amplified by multiplying this small angle by a large propagation distance. A simple minimization calculation shows that for fixed wavelength, the minimum beam size at a distance L from the focus point is $\sigma(L) \geq \sqrt{\lambda L/(2\pi)}$.

it can be seen that $w_0 = 2\sigma_0$, and in general the radial size parameter $w(z)$ is twice the transverse Gaussian width of the beam at longitudinal position z. We can now see how Eq. 18 follows from the Heisenberg uncertainty principle applied to transverse coordinates.

$$\begin{aligned}\sigma(z) = \sigma_0 \oplus \frac{\Delta p}{p} z &= \sqrt{\sigma_0^2 + \left(\frac{1/2\sigma_0}{2\pi/\lambda}\right)^2 z^2} \\ &= \sqrt{\sigma_0^2 + \left(\frac{\lambda z}{4\pi\sigma_0}\right)^2} \\ &= \sigma_0\sqrt{1 + \left(\frac{\lambda z}{4\pi\sigma_0^2}\right)^2}\end{aligned} \tag{22}$$

Inserting the factors of 2 to convert σ's into w's, we obtain the desired result

$$w(L) = w_0\sqrt{1 + \left(\frac{\lambda L}{\pi w_0^2}\right)^2} \tag{23}$$

To obtain the minimum transverse size of the beam after propagating a distance $z = L$, we can take the derivative of Eq. 23 with respect to w_0:

$$\begin{aligned}\frac{dw}{dw_0} &= \sqrt{1 + \left(\frac{\lambda L}{\pi w_0^2}\right)^2} + w_0\left(\frac{1}{2}\right)\left(\frac{1}{\sqrt{1 + \left(\frac{\lambda L}{\pi w_0^2}\right)^2}}\right)\left(\frac{\lambda L}{\pi}\right)^2(-4)\frac{1}{w_0^5} = 0 \\ &\Rightarrow 1 + \left(\frac{\lambda L}{\pi w_0^2}\right)^2 = 2\left(\frac{\lambda L}{\pi w_0^2}\right)^2 \\ &\Rightarrow w_0 = \sqrt{\frac{\lambda L}{\pi}}.\end{aligned} \tag{24}$$

Plugging this value of w_0 back into Eq. 23 gives

$$w(L) = w_0\sqrt{2} = \sqrt{\frac{2\lambda L}{\pi}}. \tag{25}$$

The transverse Gaussian width of a beam of wavelength λ therefore satisfies

$$\sigma(L) \geq \sqrt{\frac{\lambda L}{2\pi}}. \tag{26}$$

H Appendix: Computation of the power spectral density of holographic strain and phase noise

Specifically, the Hogan postulate is that information is stored on propagating null wavefronts where the minimum wavelength λ_0 is twice the Planck length $\lambda_p = \sqrt{\hbar G/c^3}$. This normalization is set by the black hole entropy-area relationship $S = A/4G = A/(2\lambda_p)^2$. If the underlying spacetime is limited by the distance scale λ_0, transverse distances between reference points become uncertain by an amount

$$\sigma(L) \geq \sqrt{\frac{\lambda_0 L}{2\pi}}. \tag{27}$$

At each roundtrip pass through the interferometer arm, the relative displacement between the beam centroid and the nominal impact position on the beam splitter is sampled from a Gaussian distribution of this width. This effect can also be viewed as a transverse jitter of the beamsplitter, with respect to the beam. Since the 45° beamsplitter couples the two transverse arms, this jitter manifests itself as a relative lengthening or shortening of the other arm, and phase noise is introduced into the interferometer.

To obtain the resulting minimum power spectral density of strain noise, we first compute the power spectral density $\Phi(f)$ of transverse displacement. The natural bandwidth from the Heisenberg uncertainty principle $\Delta f \Delta t \approx 1/2$ or equivalently the Nyquist theorem is:

$$\Delta f = \frac{1}{2\Delta t} = \frac{c}{4L} \tag{28}$$

as determined by the time $\Delta t = 2L/c$ between successive samples of the beam splitter position. The spectral density in transverse position variance is then

$$\tilde{\Xi}(f) = \frac{(\sigma(L))^2}{\Delta f} \geq \left(\frac{1}{2}\frac{\lambda_0 L}{\pi}\right)\left(\frac{4L}{c}\right) = \frac{4t_p L^2}{\pi} \tag{29}$$

where in the last equality we have substituted $\lambda_0 = 2\lambda_p = 2t_p$, the Planck time. The resulting noise in the strain $(1/L)\cdot(\Delta X - \Delta Y)/2$ receives one contribution from the transverse jitter in each arm and is given by

$$h(f) = \sqrt{\frac{1}{L^2}\cdot 2\cdot\frac{\tilde{\Xi}(f)}{4}} = \sqrt{\frac{2t_p}{\pi}}. \tag{30}$$

Plugging in $t_p = \sqrt{\hbar G/c^5} = 5.39 \times 10^{-44}$ s, we obtain

$$h(f) \geq 1.6 \times 10^{-22}/\sqrt{\text{Hz}}. \tag{31}$$

This amount is comparable to the magnitude of the mystery noise observed in the GEO600 detector, when reduced by a factor of two to account for the folding of the GEO interferometer arms.

The corresponding phase noise spectral density to be detected at the dark port of the interferometer is

$$\Phi_{\text{holo}}(f) = h(f) \cdot L \cdot \frac{2\pi}{\lambda_{\text{opt}}} \tag{32}$$

$$h(f) = \sqrt{\left(\frac{2\pi}{\lambda_{\text{opt}}}\right)^2 \cdot 2 \cdot \frac{\tilde{\Xi}(f)}{4}} = \sqrt{8\pi t_p} \cdot \frac{L}{\lambda_{\text{opt}}} \tag{33}$$

because we are now measuring jitter in units of the optical wavelength λ_{opt} instead of the arm length L. Plugging in $L = 40$ m and $\lambda_{\text{opt}} = 1.064 \times 10^{-6}$ m for our proposed experiment, we obtain

$$\Phi_{\text{holo}}(f) = 6 \times 10^{-14}/\sqrt{\text{Hz}}. \tag{34}$$

I Appendix: Safety

The experimenters are committed to following laboratory standard safety procedures and other standards found in the *Guide to Experimenters* book published by the laboratory.

I.1 Integrated Safety

We will follow the principles of integrated safety management and work with the Fermilab ES&H section to perform work safely. Certain aspects in the design such as beam tubes in 10 ft sections have been chosen in part because such a length should weigh approximately 70 lbs which is appropriate for two persons performing the assembly.

I.2 Vacuum

The vacuum system will be required to be reviewed as described in the ES&H manual, section 5033, "Vacuum Vessel Safety" which addresses a number of procedures and requirements for the design, fabrication, inspection, and test even if the vessels will be manufactured at a vendor. In addition, appropriate engineering drawings will be generated and reviewed. The overall design will include features that prevent catestrophic failures if any area is either at vacuum or is presurized such as with dry nitrogen.

I.3 Laser

The lasers intended for use will be Class IV lasers which have safety procedures documented in the ES&H manual, section 5062.1, "Lasers." The basic policy that will be followed is that no high power laser light ever be allowed to escape the apparatus and that access to any area of the apparatus where such light might exist be interlocked using failsafe techniques.

In addition, access to any area where high powered laser light might exist will require either access by key or by use of a tool. All scientific and technical personnel who will be working on the project during use of the high powered lasers will be required to go through laser safety training and suitable safety equipment such as eye protection will be available. A detailed plan will be an evolving process working with the ES&H group.

J Appendix: Response to PAC

J.1 Building a broader understanding in theoretical and experimental community

Craig Hogan has discussed the holographic noise models in a number of conference and workshop settings. There is widespread interest in the possibility of an experiment, but the connection of the effective theory used here with frontier fundamental unification theories based on strings, matrices, or loops remains, at this stage, heuristic. Even though black hole entropy allows an absolute calibration of holographic uncertainty within the context of the effective theory, there is no standard physical interpretation of the holographic principle in terms of fundamental microscopic degrees of freedom that can be used to calculate holographic noise. Indeed, there is no consensus on the physical interpretation of a minimum time or maximum frequency, the basic postulates used here.

One reason for this disconnect is that the best understood results in holographic unification refer to global mappings, in contrast to the formulation here that necessarily connects with local observables. For example, the most precise and well-controlled results in holographic unification are associated with dualities between systems of bulk fields with gravity in highly curved Anti-de Sitter space, and conformal field theories on the lower-dimensional boundary. There is no similar dual known for familiar types of quantum states in a nearly-flat spacetime. However, since the field is data-starved, results from any new experiment with Planck sensitivity should be of broad interest to those seeking insights about the macroscopic interpretation of holography.

Both the GEO600 and LIGO communities are aware of the predicted holographic noise, as a possible limitation to certain configurations of gravity wave detectors. GEO600 is actively trying to understand their noise sources and plans to publish an experimental result on holographic noise. LIGO plans to publish a correlation measurement between two nearby interferometers which formally has Planck sensitivity in strain units, although it has less sensitivity to the predicted holographic noise.

J.2 Critical Review by outside experts

A project review including external experts from the experimental gravitational wave community, as well as internal theorists, will be conducted on November 3, 2009. The results of the review will be made available to the PAC.

J.3 Design level to evaluate cost and risk

The experiment has been designed to minimize cost and technical risk. Because the apparatus does not need to be optimized to see low frequency, low duty cycle gravity wave signals from astrophysical events, the required phase sensitivity is orders of magnitude less than that achieved by LIGO and GEO. The holographic signal has a broadband spectrum, and it is always present. Therefore, lower fluxes of photons can be used, combined with longer integration times. The devices are expected to be constructed from conventional parts, mostly off-the-shelf, with a few special order optics items which are far from the state-of-the-art technology. The measurement will be performed at high (MHz) frequencies, well above the sub-kHz frequencies of the environmental noise which plagues gravity wave detectors which must search for signals at these low frequencies. Finally, the ability to turn the correlated signal on and off by separating the interferometers provides a useful experimental knob to validate the signal. These features are documented elsewhere in this proposal.

J.4 Technical collaboration with GEO600 and the large interferometers

The experimental collaboration includes several members of LIGO who have contributed their technical expertise to the design and costing of the experiment. They will continue to participate in the construction, commissioning, and science. Members of GEO600 are participating in technical reviews of the project, are are sharing recent progress in understanding their mystery noise on an ongoing basis.